Composite Structures 159 (2017) 548–566

Contents lists available at ScienceDirect

Composite Structures

journal homepage: www.elsevier.com/locate/compstruct

Eigenvalue buckling analysis of cracked functionally graded cylindrical shells in the framework of the extended finite element method

Amir Nasirmanesh, Soheil Mohammadi *

High Performance Computing Lab, School of Civil Engineering, University of Tehran, Tehran, Iran

ARTICLE INFO

Article history:
Received 19 June 2016
Revised 17 September 2016
Accepted 22 September 2016
Available online 23 September 2016

Keywords:
Buckling
Cylindrical shell
Extended finite element method (XFEM)
Crack
Functionally graded material (FGM)

ABSTRACT

In this study, eigenvalue buckling analysis for cracked functionally graded cylindrical shells is performed using eight noded degenerated shell elements in the framework of the extended finite element method. First, validity and efficiency of the proposed method in comparison with available results are examined and then the approach is utilized for examining cracked FGM cylindrical shells subjected to different loading conditions, including axial compression, axial tension and combined internal pressure and axial compression. Also, the effects of various parameters such as crack length and angle, gradient index of the material, aspect ratio of the cylinder and internal pressure on the buckling behavior are extensively investigated.

1. Introduction

Composite shell structures have been extensively utilized for a broad range of applications including space crafts, airplane fuselage, thermal coating barriers, defense systems and many others due to their considerably high strength to weight ratio. Nevertheless, fiber reinforced laminate shells suffer from many disadvantages such as delamination vulnerability to impact loading, low resistance to sustain in thermal environments. Functionally graded materials are a new class of composite materials which have obviated the interface-related problems in traditionally laminate composites due to their continuous and smooth variation of materials across the thickness. Usually, these materials consist of a ceramic surface, which can be imposed to a high gradient of thermal loading, gradually changed into a metallic surface on the other side to withstand in mechanical loadings. As a result, functionally graded cylindrical shells have drawn special attention from the application and theoretical points of view. Despite their superior characteristics, there are several failure modes which may endanger the overall safety of these structures. Among them, buckling can be one of the dominant failure modes. On the other hand, because functionally graded materials are often used in extreme environments, they are highly prone to imperfections such as voids and cracks in their structure during the production and life service. Hence, it is vital to perform accurate buckling analyses for cracked functionally graded cylindrical shells to allow for better and more reliable designs.

Many comprehensive studies have been performed on the buckling behavior of functionally graded cylindrical shells in the past decade. Ng et al. [1] presented an analytical formulation for dynamic buckling behavior of FGM cylindrical shells subjected to periodic loadings. They found out that the gradient index of the material could crucially affect the buckling behavior of the problem. Another analytical solution was presented by Sofiyev [2] concerning the buckling analysis of FGM cylindrical shells subjected to axial dynamic loadings. Further analytical studies for buckling and postbuckling of functionally graded cylindrical shells can be found in [3–10].

On the other hand, there are only limited works on the buckling of cracked cylindrical shells. Esteknachi and Vafai [11] studied the buckling behavior of isotropic cracked cylindrical shells subjected to axial loading using the classical finite element method. They used a mesh zooming scheme for adaptive generation of the mesh of the cylindrical shell so that with approaching to the crack tip the size of the elements would decrease from the standard size of the uncracked regions to a very finer size to better capture the crack tip stress singularity. They also performed a similar study for cracked plates [12]. The effect of internal pressure on the buckling behavior of cracked cylindrical shells subjected to combined internal pressure and axial compression was investigated by Vaziri and Estekanchi [13] using the commercial FEM package ANSYS. They concluded that the effect of the internal pressure on the buckling stresses became completely different depending on the crack being

* Corresponding author.
E-mail address: smoham@ut.ac.ir (S. Mohammadi).

http://dx.doi.org/10.1016/j.compstruct.2016.09.065
0263-8223/

axial or circumferential. For instance, when the crack was in the axial direction of the cylinder, the internal pressure had a detrimental effect on the buckling stresses, whereas, for the circumferential crack, the internal pressure had a stabilizing effect on the buckling behavior [13]. Also, Vaziri [14] carried out a linear eigenvalue buckling analysis using the finite element method to study the effect of crack length, crack orientation and the sequence of the lamina on the buckling behavior of composite cylindrical shells under axial compression. Dynamic stability and vibration of cracked cylindrical shells under compressive and tensile periodic loadings were investigated using the finite element method by Javidruzi et al. [15]. They showed that the existence of crack could considerably decrease the natural frequency of the shell. Also, Tafreshi [16–18] performed a series of delamination buckling and postbuckling analysis for laminate composite cylindrical shells under various loading conditions by the finite element method.

In addition, there are a few works which have addressed the buckling analysis of cracked plates in the framework of the extended finite element method. Recently, Nasirmanesh and Mohammadi [19] performed an eigenvalue buckling analysis for cracked composite plates using the extended finite element method. They examined several problems and thoroughly investigated the effects of different parameters such as crack lengths, crack angles and direction of fibers on the buckling behavior of composite plates. They also concluded that even for the tensile loading, changes in the fiber direction can alter the local instability around the crack faces to a global buckling mode.

Natarajan et al. [20] carried out thermo-mechanical buckling analysis of cracked functionally graded plates in the framework of the partition of unity method and examined the effects of gradient index of the material and crack lengths on the critical temperature and critical buckling stresses. Another XFEM buckling analysis for cracked FGM rectangular plates subjected to compressive loading was reported by Liu et al. [21]. Baiz et al. [22] used the smooth curvature method to study the effects of crack lengths and locations on the critical buckling stresses for isotropic plates. None of the existing works have studied the buckling behavior of cracked functionally graded shells. The novelty of the present study is, for the first time, to propose an XFEM shell formulation to carry out an eigenvalue buckling analysis for cracked FGM cylindrical shells.

XFEM was motivated by disadvantages of the classical finite element method for fracture analysis; including the need for mesh conformity to crack path and incapability to capture the exact stress field near a crack tip. In XFEM, while cracks are represented independent of the mesh, the exact analytical stress field around the crack tip is achieved. The method has been extended to static and dynamic orthotropic problems for both fixed and propagating cracks [23–30], bi-materials [31,32] and FGMs [33]. Recently, Rashetnia and Mohammadi [34] proposed a new set of tip enrichment functions for studying the fracture behavior of rubber-like materials which experience large deformations. They concluded that the logarithmic set of enrichment functions are more accurate and efficient.

There are other approaches that are capable of handling complex problems including nonlinear dynamic fracture and fluid driven fracture of plates and shells. For instance, Nguyen-Thanh et al. [35] proposed a model based upon the extended isogeometric method in accordance with the Kirchhoff-Love theory to analyze thin shells. In addition, a meshfree method was proposed for nonlinear dynamic fracture analysis of thin shells, which allowed to predict crack propagation across the thickness of shell [36,37]. Recently, the phase-field method has been utilized to study the fracturing behavior of plates and shells [38,39] with the goal of avoiding explicit track of cracks in special problems.

The present paper is organized as follows: the basic formulation of the functionally graded problem is presented. Definition of degenerated shell elements is followed by deriving the stability equations in the framework of the extended finite element method. Numerical simulations are presented and discussed for verifying the proposed method and then extended to cracked FGM problems in Section 3. Finally, a brief review of the concluding remarks is presented.

2. Theoretical formulation and XFEM discretization

In this study, the Young's module (E_z) of the problem is assumed to vary across the thickness; from the pure metallic surface at the bottom (E_m) to the fully ceramic surface at the top (E_c) of the shell based on a power distribution law,

$$E_z = E_m + (E_c - E_m)\left(\frac{1}{2}+\frac{z}{t}\right)^n \tag{1}$$

where t is the thickness of shell, n is the gradient index of the material and z changes along the thickness so that $-t/2 \leqslant z \leqslant t/2$, as shown in Fig. 1. The Poisson's ratio v, however, is assumed constant.

In order to avoid mesh distortion and shear locking that usually occur in buckling phenomena, 8-noded shell elements are adopted to discretize the domain [19,40]. Geometry of the shell is defined using the coordinates of the mid-surface of the shell and the unit normal vector, which is perpendicular to the surface of the shell at each node, $\mathbf{V}_i^3$, as depicted in Fig. 2,

$$\mathbf{x} = \sum_{i=1}^{8} N_i \mathbf{x}_i + \sum_{i=1}^{8} \frac{t_i \zeta_i}{2} N_i \mathbf{V}_i^3; \quad \mathbf{x} = \{x, y, z\}^T \tag{2}$$

where, N_i's are the shape functions of the plane eight noded element, t_i is the thickness of the shell at each node (which is assumed constant in all nodes in this study) and ζ of the natural coordinate system is perpendicular to the surface of the shell at each node.

Consider a cracked FGM medium, depicted in Fig. 3, the displacement field of the problem in the framework of the extended finite element method is presented as

$$\mathbf{u} = \begin{Bmatrix} u \\ v \\ w \end{Bmatrix} = \mathbf{u}_{FE} + \mathbf{u}_{Enr} \tag{3}$$

where, u, v and w are the displacement components in the global coordinate x, y and z directions, respectively. $\mathbf{u}_{FE}$ and $\mathbf{u}_{Enr}$ are the conventional continuous finite element approximation and the approximation of the discontinuous part of the displacements, respectively. $\mathbf{u}_{FE}$ can be written as,

$$\mathbf{u}_{FE} = \sum_{i=1}^{8} N_i \begin{Bmatrix} u_i \\ v_i \\ w_i \end{Bmatrix} + \sum_{i=1}^{8} \frac{t\zeta_i}{2} N_i \left\{ \beta_i \begin{Bmatrix} e_{y1}^i \\ e_{y2}^i \\ e_{y2}^i \end{Bmatrix} - \alpha_i \begin{Bmatrix} e_{x1}^i \\ e_{x2}^i \\ e_{x3}^i \end{Bmatrix} \right\} \tag{4}$$

where e_{yk}^i and e_{xk}^i are the components of the unit orthonormal vectors of the unit normal vector at node i, i.e. $\mathbf{V}_i^3$. α_i and β_i are the rotational degrees of freedom with respect to x and y axes, respectively.$\mathbf{u}_{Enr}$ is composed of two separate parts to account for discontinuous and singular fields; each part enriches the displacement field with specific enrichment functions to overcome the limitation of the conventional finite element method. As a result, neither the mesh conformity to the crack edges nor the mesh refinement around the crack tip is required.

$$\mathbf{u}_{Enr} = \mathbf{u}_{Heaviside} + \mathbf{u}_{Tip} \tag{5}$$

$$\mathbf{u}_{Heaviside} = \sum_{i=1}^{8} N_i H(\mathbf{x}) \begin{Bmatrix} a_1^i \\ a_2^i \\ a_3^i \end{Bmatrix} + \sum_{i=1}^{8} \frac{t\zeta_i}{2} N_i H(\mathbf{x}) \left\{ a_\beta^i \begin{Bmatrix} e_{y1}^i \\ e_{y2}^i \\ e_{y2}^i \end{Bmatrix} - a_\alpha^i \begin{Bmatrix} e_{x1}^i \\ e_{x2}^i \\ e_{x3}^i \end{Bmatrix} \right\} \tag{6}$$

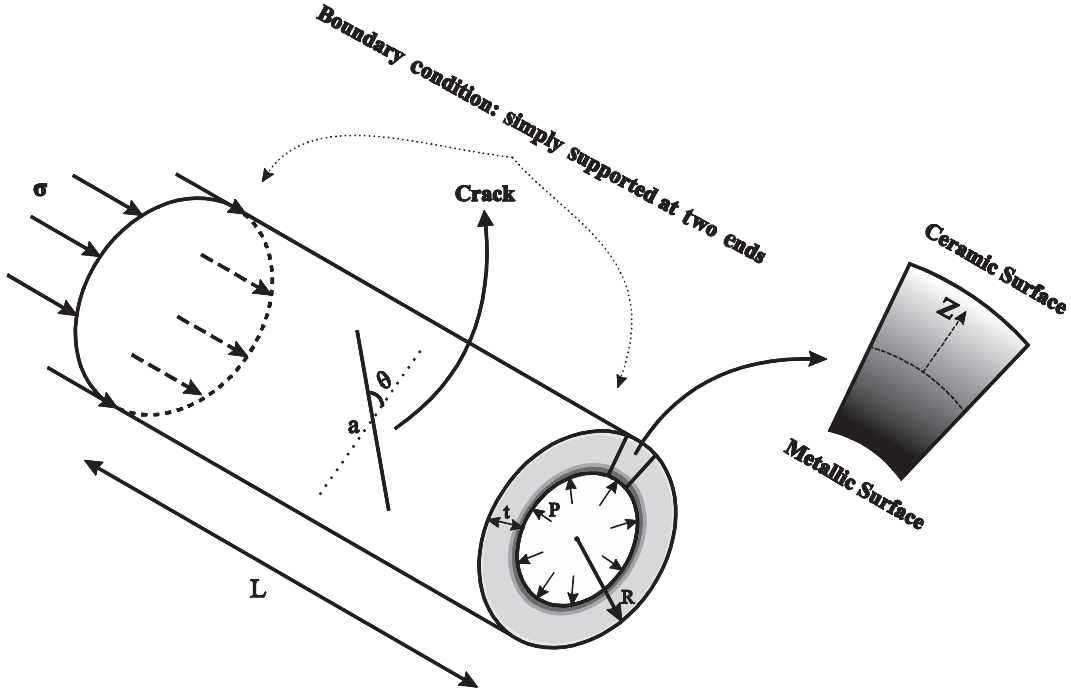

Fig. 1. Geometry of the cracked cylindrical shell and variation of material properties across the thickness.

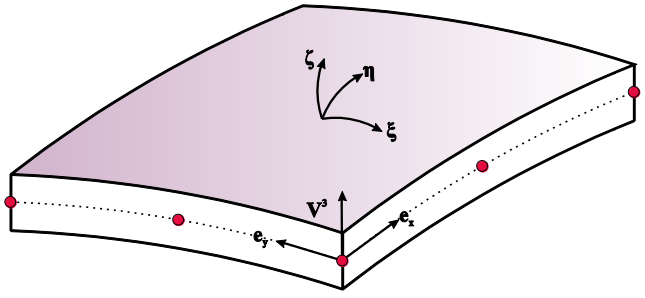

Fig. 2. Eight noded shell element and local unit vectors.

$$\mathbf{u}_{\mathrm{Tip}}=\sum_{i=1}^{8}N_i\sum_{j=1}^{4}(F_j(\mathbf{x})-F_j(\mathbf{x}_j))\begin{Bmatrix}b_1^i\\b_2^i\\0\end{Bmatrix}+\sum_{i=1}^{8}N_i\sum_{j=1}^{1}(G_j(\mathbf{x})-G_j(\mathbf{x}_j))\begin{Bmatrix}0\\0\\b_3^i\end{Bmatrix}+\sum_{i=1}^{8}\frac{t\zeta_i}{2}N_i\sum_{j=1}^{4}(R_j(\mathbf{x})-R_j(\mathbf{x}_j))\left\{b_{\beta j}^i\begin{Bmatrix}e_{y1}^i\\e_{y2}^i\\e_{y2}^i\end{Bmatrix}-b_{\alpha j}^i\begin{Bmatrix}e_{x1}^i\\e_{x2}^i\\e_{x2}^i\end{Bmatrix}\right\}\tag{7}$$

where, a_j^i and b_j^i are the additional enrichment degrees of freedom. The vector of nodal displacements (**d**) and enrichments (**h** and **t**) are defined as

$$\mathbf{d}=\{u,v,w,\alpha,\beta\}^T\tag{8}$$

$$\mathbf{h}=\{a_1,a_2,a_3,a_\alpha,a_\beta\}^T\tag{9}$$

$$\mathbf{t}=\{b_1,b_2,b_3,b_\alpha,b_\beta\}^T\tag{10}$$

and the vector of unknowns **D**,

$$\mathbf{D}=\{\mathbf{d}\ \mathbf{h}\ \mathbf{t}_1\ \mathbf{t}_2\ \mathbf{t}_3\ \mathbf{t}_4\}^T\tag{11}$$

In Eq. (6), $H(\mathbf{x})$ is the Heaviside function and is defined as [41]

$$H(\mathbf{x})=\begin{cases}+1 & \mathbf{x}\text{ above the crack}\\ -1 & \mathbf{x}\text{ under the crack}\end{cases}\tag{12}$$

Also, the in-plane, out of plane and rotational enrichment functions in the local polar coordinate system (r,θ) are expressed as [40],

$$F(r,\theta)=\left\{\sqrt{r}\sin\left(\frac{\theta}{2}\right),\sqrt{r}\cos\left(\frac{\theta}{2}\right),\sqrt{r}\sin\left(\frac{\theta}{2}\right)\sin(\theta),\sqrt{r}\cos\left(\frac{\theta}{2}\right)\sin(\theta)\right\}\tag{13}$$

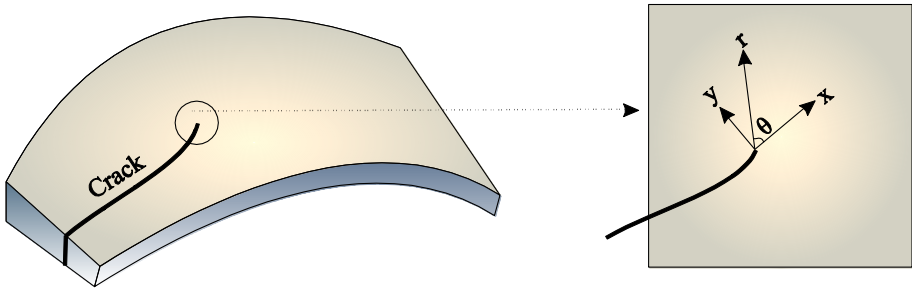

Fig. 3. Cracked medium and local crack tip coordinates.

$$G(r,\theta)=\left\{\sqrt{r}\sin\left(\frac{\theta}{2}\right)\right\} \tag{14}$$

$$R(r,\theta)=\left\{\sqrt{r}\sin\left(\frac{\theta}{2}\right),\sqrt{r}\cos\left(\frac{\theta}{2}\right),\sqrt{r}\sin\left(\frac{\theta}{2}\right)\sin(\theta),\sqrt{r}\cos\left(\frac{\theta}{2}\right)\sin(\theta)\right\} \tag{15}$$

To obtain the governing equations, the total potential energy is written as:

$$\psi=\prod_b+\prod_\sigma-\prod_\Omega \tag{16}$$

where $\prod_b$ is the bending strain energy and $\prod_\sigma$ represents the membrane energy, necessary in buckling problems [42] and $\prod_\Omega$ is the potential of external loads.

$$\prod_b=\frac{1}{2}\int_v \varepsilon_L^T\mathbf{C}\varepsilon_L dV \tag{17}$$

$$\prod_\sigma=\int_v \varepsilon_{NL}^T\sigma_0 dV \tag{18}$$

$$\prod_\Omega=\int_v \mathbf{u}^T\mathbf{q}dV \tag{19}$$

where σ_0 is the tensor of initial stresses, which is computed from a static analysis, $\mathbf{C}$ is the matrix of the material property, $\mathbf{q}$ is the traction tensor, and ε_L & ε_{NL} are the linear and nonlinear terms of the Green-Lagrange strains, respectively,

$$\varepsilon_L=\left\{\frac{\partial u}{\partial x},\frac{\partial v}{\partial y},\frac{\partial w}{\partial z},\frac{\partial v}{\partial x}+\frac{\partial u}{\partial y},\frac{\partial w}{\partial y}+\frac{\partial v}{\partial z},\frac{\partial u}{\partial z}+\frac{\partial w}{\partial x}\right\}^T \tag{20}$$

$$\varepsilon_{NL}=\begin{Bmatrix}\frac{1}{2}\left(\frac{\partial u}{\partial x}\right)^2+\frac{1}{2}\left(\frac{\partial v}{\partial x}\right)^2+\frac{1}{2}\left(\frac{\partial w}{\partial x}\right)^2\\ \frac{1}{2}\left(\frac{\partial u}{\partial y}\right)^2+\frac{1}{2}\left(\frac{\partial v}{\partial y}\right)^2+\frac{1}{2}\left(\frac{\partial w}{\partial y}\right)^2\\ \frac{1}{2}\left(\frac{\partial u}{\partial z}\right)^2+\frac{1}{2}\left(\frac{\partial v}{\partial z}\right)^2+\frac{1}{2}\left(\frac{\partial w}{\partial z}\right)^2\\ \frac{\partial u}{\partial x}\frac{\partial u}{\partial y}+\frac{\partial v}{\partial x}\frac{\partial v}{\partial y}+\frac{\partial w}{\partial x}\frac{\partial w}{\partial y}\\ \frac{\partial u}{\partial y}\frac{\partial u}{\partial z}+\frac{\partial v}{\partial y}\frac{\partial v}{\partial z}+\frac{\partial w}{\partial y}\frac{\partial w}{\partial z}\\ \frac{\partial u}{\partial z}\frac{\partial u}{\partial x}+\frac{\partial v}{\partial z}\frac{\partial v}{\partial x}+\frac{\partial w}{\partial z}\frac{\partial w}{\partial x}\end{Bmatrix} \tag{21}$$

$$\sigma_0=\{\sigma_{x0},\sigma_{y0},\sigma_{z0},\tau_{xy0},\tau_{yz0},\tau_{xz0}\}^T \tag{22}$$

Also, strain and stress tensors are related by the tensor of material properties $\mathbf{C}$,

$$\sigma=\mathbf{C}\varepsilon \tag{23}$$

$$\mathbf{C}=\begin{bmatrix}C_{11}&C_{12}&C_{12}&0&0&0\\C_{12}&C_{11}&C_{12}&0&0&0\\C_{12}&C_{12}&C_{11}&0&0&0\\0&0&0&C_{44}&0&0\\0&0&0&0&C_{44}&0\\0&0&0&0&0&C_{44}\end{bmatrix} \tag{24}$$

where C_{ij} components depend only to the modulus of elasticity E_z and the Poisson's ratio v of the material,

$$C_{11}=\frac{E_z}{1-v^2},\ C_{12}=\frac{vE_z}{1-v^2},\ C_{44}=\frac{E_z}{2(1+v)} \tag{25}$$

Eq. (18) can be rewritten as:

$$\prod_\sigma=\frac{1}{2}\int_v \mu^T\mathbf{S}_0\mu dV \text{ where } \mu=\{\mathbf{u}_{,x}\ \mathbf{u}_{,y}\ \mathbf{u}_{,z}\ \mathbf{v}_{,x}\ \mathbf{v}_{,y}\ \mathbf{v}_{,z}\ \mathbf{w}_{,x}\ \mathbf{w}_{,y}\ \mathbf{w}_{,z}\}^T \tag{26}$$

$\mathbf{S}_0$ is computed from the stresses obtained from the first stage of the buckling analysis; a static analysis,

$$\mathbf{S}_0=\begin{bmatrix}\hat{\mathbf{S}}_0&\mathbf{0}&\mathbf{0}\\\mathbf{0}&\hat{\mathbf{S}}_0&\mathbf{0}\\\mathbf{0}&\mathbf{0}&\hat{\mathbf{S}}_0\end{bmatrix};\quad \hat{\mathbf{S}}_0=\begin{bmatrix}\sigma_x^0&\tau_{xy}^0&\tau_{xz}^0\\\tau_{xy}^0&\sigma_y^0&\tau_{yz}^0\\\tau_{xz}^0&\tau_{yz}^0&\sigma_z^0\end{bmatrix} \tag{27}$$

Vectors of $\varepsilon_L\mu$ and $\mathbf{u}$ are related to the nodal displacement vector $\mathbf{D}$ as

$$\varepsilon_L=\mathbf{B}\mathbf{D},\ \ \mu=\mathbf{B}_G\mathbf{D} \text{ and } \mathbf{u}=\mathbf{N}\mathbf{D} \tag{28}$$

where $\mathbf{B}$ and $\mathbf{B}_G$ correspond to linear and nonlinear parts of the Green-Lagrange strain, respectively [19], and $\mathbf{N}$ is constructed from the shape functions as

$$\mathbf{N}_i^{r/s}=\begin{bmatrix}\phi_i&0&0&-\frac{\zeta_i t}{2}e_{x1}\varphi_i&\frac{\zeta_i t}{2}e_{y1}\varphi_i\\0&\phi_i&0&-\frac{\zeta_i t}{2}e_{x2}\varphi_i&\frac{\zeta_i t}{2}e_{y2}\varphi_i\\0&0&\kappa_i&-\frac{\zeta_i t}{2}e_{x3}\varphi_i&\frac{\zeta_i t}{2}e_{y3}\varphi_i\end{bmatrix} \tag{29}$$

Substituting Eq. (28) into Eqs. (17), (18) and (19), the total potential energy becomes

$$\psi=\frac{1}{2}\int_V \mathbf{D}^T\mathbf{B}^T\mathbf{C}\mathbf{B}\mathbf{D}dV+\frac{1}{2}\int_V \mathbf{D}^T\mathbf{B}_G^T\mathbf{S}_0\mathbf{B}_G\mathbf{D}dV-\int_V \mathbf{D}^T\mathbf{q}dV \tag{30}$$

Based on the principle of minimum potential energy, variation of the total potential energy must vanish at equilibrium ($\delta\psi=0$),

$$\delta\psi=\delta\mathbf{D}\left\{\left(\int_V \mathbf{B}^T\mathbf{C}\mathbf{B}dV+\int_V \mathbf{B}_G^T\mathbf{S}_0\mathbf{B}_G dV\right)\mathbf{D}-\int_V \mathbf{N}^T\mathbf{q}dV\right\}=0\quad \forall\delta\mathbf{D}\neq 0 \tag{31}$$

Applying the XFEM displacement approximation (3), the following equilibrium state is obtained after some manipulation and simplification [42]

$$\{\mathbf{K}+\mathbf{K}_\mathbf{G}\}\{\mathbf{D}\}=\mathbf{F}_{\text{ext}} \tag{32}$$

where $\mathbf{K}$ and $\mathbf{K}_\mathbf{G}$ are the conventional and geometric stiffness matrices, respectively, and $\mathbf{F}_{\text{ext}}$ is the vector of external forces.

For a linear problem, if the external load vector is multiplied by a factor λ, then, the geometric stiffness matrix is also multiplied by λ,

$$\{\mathbf{K}+\lambda\mathbf{K}_\mathbf{G}\}\{\mathbf{D}\}=\lambda\mathbf{F}_{\text{ext}} \tag{33}$$

Having the definition of buckling by Cook [42], when buckling occurs, the external load does not change for an infinitesimal displacement of $d\mathbf{D}$,

$$\{\mathbf{K}+\lambda\mathbf{K}_\mathbf{G}\}\{\mathbf{D}+d\mathbf{D}\}=\lambda\mathbf{F}_{\text{ext}} \tag{34}$$

Subtracting Eq. (34) from Eq. (35) leads to the stability equation of the problem,

$$\{\mathbf{K}+\lambda\mathbf{K}_\mathbf{G}\}\{d\mathbf{D}\}=0 \tag{35}$$

where λ is the eigenvalue of the system. The buckling stress is obtained by multiplying λ to the initial external stress of the system, and the minimum value of λ corresponds to the critical buckling stress of the system. For any specified value of λ, there is an eigenvector $d\mathbf{D}$ which represents the buckling mode shape of the problem.

$$\mathbf{K}_{ij}^{rs}=\int_v (\mathbf{B}_i^r)^T\mathbf{C}(\mathbf{B}_j^s)dV \tag{36}$$

$$\mathbf{K}_{Gij}^{rs}=\int_v (\mathbf{B}_{Gi^r}^T)\mathbf{S}_0(\mathbf{B}_{Gj^s})dV\quad (r,s=\mathbf{d},\mathbf{h},\mathbf{t}) \tag{37}$$

$$\mathbf{F}_{\text{exti}}^{rs}=\int_V (\mathbf{N}_i^{rs})^T\mathbf{q}dV \tag{38}$$

For facilitating the construction of $\mathbf{B}_i^{r/s}$, $\mathbf{B}_{Gi}^{r/s}$ and $\mathbf{N}_i^{r/s}$ for different $r,s=\mathbf{d},\mathbf{h},\mathbf{t}$, the following functions are defined

$$\begin{aligned}\phi &= N_i(F_j(\mathbf{x})-F_j(\mathbf{x}_i))\\ \varphi &= N_i(R_j(\mathbf{x})-R_j(\mathbf{x}_i))\\ \kappa &= N_i(G_j(\mathbf{x})-G_j(\mathbf{x}_i))\end{aligned} \tag{39}$$

So

$$\mathbf{B}_i^{r/s}=\begin{bmatrix} \phi_{i,x} & 0 & 0 & \left(-\frac{\zeta_i t}{2}e_{x1}\varphi_i\right)_{,x} & \left(\frac{\zeta_i t}{2}e_{y1}\varphi_i\right)_{,x}\\ 0 & \phi_{i,y} & 0 & \left(-\frac{\zeta_i t}{2}e_{x2}\varphi_i\right)_{,y} & \left(\frac{\zeta_i t}{2}e_{y2}\varphi_i\right)_{,y}\\ 0 & 0 & \kappa_{i,z} & \left(-\frac{\zeta_i t}{2}e_{x3}\varphi_i\right)_{,z} & \left(\frac{\zeta_i t}{2}e_{y3}\varphi_i\right)_{,z}\\ & & & \left(-\frac{\zeta_i t}{2}e_{x1}\varphi_i\right)_{,y}+ & \left(\frac{\zeta_i t}{2}e_{y1}\varphi_i\right)_{,y}\\ \phi_{i,y} & \phi_{i,x} & 0 & \left(-\frac{\zeta_i t}{2}e_{x2}\varphi_i\right)_{,x} & +\left(\frac{\zeta_i t}{2}e_{y2}\varphi_i\right)_{,x}\\ & & & \left(-\frac{\zeta_i t}{2}e_{x2}\varphi_i\right)_{,z} & \left(\frac{\zeta_i t}{2}e_{y2}\varphi_i\right)_{,z}+\\ 0 & \phi_{i,z} & \kappa_{i,y} & +\left(-\frac{\zeta_i t}{2}e_{x3}\varphi_i\right)_{,y} & \left(\frac{\zeta_i t}{2}e_{y3}\varphi_i\right)_{,y}\\ & & & \left(-\frac{\zeta_i t}{2}e_{x1}\varphi_i\right)_{,z}+ & \left(\frac{\zeta_i t}{2}e_{y1}\varphi_i\right)_{,z}+\\ \phi_{i,z} & 0 & \kappa_{i,x} & \left(-\frac{\zeta_i t}{2}e_{x3}\varphi_i\right)_{,x} & \left(\frac{\zeta_i t}{2}e_{y3}\varphi_i\right)_{,x}\end{bmatrix} \tag{40}$$

$$\mathbf{B}_{Gi}^{r/s}=\begin{bmatrix} \phi_{i,x} & 0 & 0 & \left(-\frac{\zeta_i t}{2}e_{x1}\varphi_i\right)_{,x} & \left(\frac{\zeta_i t}{2}e_{y1}\varphi_i\right)_{,x}\\ \phi_{i,y} & 0 & 0 & \left(-\frac{\zeta_i t}{2}e_{x1}\varphi_i\right)_{,y} & \left(\frac{\zeta_i t}{2}e_{y1}\varphi_i\right)_{,y}\\ \phi_{i,z} & 0 & 0 & \left(-\frac{\zeta_i t}{2}e_{x1}\varphi_i\right)_{,z} & \left(\frac{\zeta_i t}{2}e_{y1}\varphi_i\right)_{,z}\\ 0 & \phi_{i,x} & 0 & \left(-\frac{\zeta_i t}{2}e_{x2}\varphi_i\right)_{,x} & \left(\frac{\zeta_i t}{2}e_{y2}\varphi_i\right)_{,x}\\ 0 & \phi_{i,y} & 0 & \left(-\frac{\zeta_i t}{2}e_{x2}\varphi_i\right)_{,y} & \left(\frac{\zeta_i t}{2}e_{y2}\varphi_i\right)_{,y}\\ 0 & \phi_{i,z} & 0 & \left(-\frac{\zeta_i t}{2}e_{x2}\varphi_i\right)_{,z} & \left(\frac{\zeta_i t}{2}e_{y2}\varphi_i\right)_{,z}\\ 0 & 0 & \kappa_{i,x} & \left(-\frac{\zeta_i t}{2}e_{x3}\varphi_i\right)_{,x} & \left(\frac{\zeta_i t}{2}e_{y3}\varphi_i\right)_{,x}\\ 0 & 0 & \kappa_{i,y} & \left(-\frac{\zeta_i t}{2}e_{x3}\varphi_i\right)_{,y} & \left(\frac{\zeta_i t}{2}e_{y3}\varphi_i\right)_{,y}\\ 0 & 0 & \kappa_{i,z} & \left(-\frac{\zeta_i t}{2}e_{x3}\varphi_i\right)_{,z} & \left(\frac{\zeta_i t}{2}e_{y3}\varphi_i\right)_{,z}\end{bmatrix} \tag{41}$$

$$\begin{cases} if: r/s=\mathbf{d}\longrightarrow \phi=\varphi=\kappa=N_i\\ if: r/s=\mathbf{h}\longrightarrow \phi=\varphi=\kappa=N_i(H(\mathbf{x})-H(\mathbf{x}_i))\\ if: r/s=\mathbf{t}\longrightarrow \phi,\varphi,\kappa=\text{as defined in equation (33)}\end{cases} \tag{42}$$

It should be noted that because of the highly complex stress field around the crack tip and the displacement discontinuity across the crack faces, the conventional Gauss quadrature integration technique is not adequate to properly evaluate the integrals of Eqs. (36), (37) and (38). In this study, the sub-triangulation method along with the Gauss quadrature rule is adopted due to its simplicity and acceptable accuracy [21–23]. In this approach, 13 Gauss points per triangle are considered for elements enriched by the tip enrichment functions, while, for split elements, 7 Gauss points are adopted per triangle, and a simple 2×2 Gauss quadrature rule is used for the standard ordinary elements, as depicted in Fig. 4.

3. Numerical simulations

In this section, linear eigenvalue buckling analysis is performed for several mixed-mode cracked homogeneous and inhomogeneous FGM plates and cylindrical shells in the framework of the extended finite element method. Due to the fact that there is no published document on the buckling of cracked functionally graded cylindrical shells, first, a problem of cracked FGM plate under compressive loading is analyzed to show the capability of the proposed method and to perform the required comparisons. Then, buckling of a cracked isotropic cylindrical shell under combined internal pressure and compressive loading as well as pure axial tension is investigated and the obtained results are verified with available studies. Afterward, a perfect functionally graded cylindrical shell subjected to axial compression is adopted and the predicted buckling stresses are compared with the available results. A thorough study is then carried out on the buckling behavior of mixed-mode cracked functionally graded cylindrical shells subjected to three different cases of loading including axial tension, axial compression and combined internal pressure and axial compression. In addition, the effect of different parameters such as crack lengths, crack angles, gradient index of the material, thickness and the aspect ratios of the shell on the buckling behavior are extensively discussed. Finally, because the proposed XFEM approach can handle the problems with multiple cracks without any additional complexity, the buckling analysis is performed on a compressive FGM cylindrical shell with three parallel cracks.

3.1. Cracked FGM rectangular plate subjected to uniaxial compressive loading

As the first example, a central cracked FGM rectangular plate under compression, as depicted in Fig. 5, is considered. It is assumed that the elasticity modulus of the plate varies through the thickness based on a power distribution law, from the fully metallic surface in the bottom to the fully ceramic in the top sur-

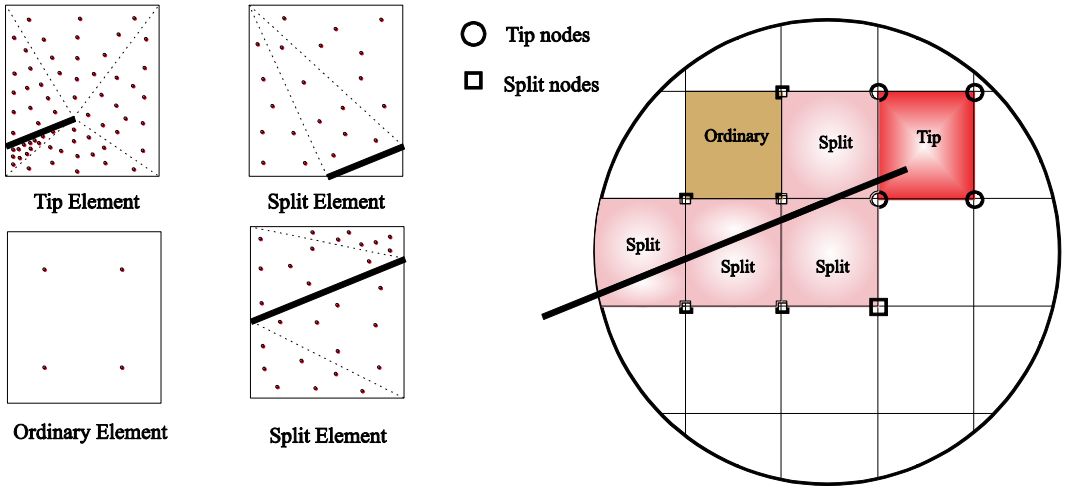

Fig. 4. Element types and their associated enriched nodes, triangulation and Gauss points.

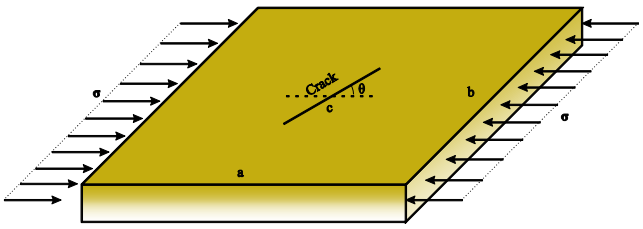

Fig. 5. A central cracked FGM plate under compression.

face of the plate. This problem has recently been studied by a so-called stabilized discrete shear gap extended 3-node triangular plate element [21]. The young's modulus is $E_m = 70 \times 10^9$ MPa and $E_c = 151 \times 10^9$ MPa on metallic and ceramic surfaces, respectively. Also, the constant Poisson's ratio of 0.3 is assumed through the thickness.

A 35×35 structured mesh is adopted for the eigenvalue buckling analysis and the computed critical buckling stresses are normalized by the parameter $k_{uni} = 12(1-\nu^2)\sigma_x^0 \lambda_{cr} b^2/\pi^2 t^3 E_c$. The aspect ratio of the plate, thickness, crack length and the angle of the crack are adopted as $a/b = 1$, $t/a = 0.01$, $c/a = 0.6$ and $\theta = 0^\circ$, respectively.

Computed normalized buckling parameters for different values of gradient index of the material are shown in Table 1. It is observed that the buckling stress decreases as the gradient index of the material increases. Also, very close results to Ref. [21] are obtained; showing sufficient accuracy for modeling the buckling behavior of cracked functionally graded plates.

3.2. Cracked homogeneous cylindrical shells

3.2.1. Simultaneous internal pressure and axial compression

As the second example, the problem of buckling of a cracked homogeneous isotropic cylindrical shell for two different loading conditions; including combined internal pressure and axial compression and pure axial tension, is considered. This problem was earlier investigated comprehensively by Vaziri and Estekanchi [13] and Seifi et al. [43] using commercial finite element analysis programs. Very fine meshes were adopted to model the stress concentration at the crack tips. In the present study, the stress singularity at crack tips is captured in a more accurate manner using the tip enrichment functions. Then, the bifurcation buckling analysis is performed in the framework of the extended finite element method.

First, the same problem of [13] is considered (Fig. 1). Material and geometric properties of the problem are $E = 69$ GPa, $\nu = 0.3$, $L = 2$ m, $R = 0.5$ m and $t = 0.5$ mm. Here, only a comparison is made between the results of the present XFEM and the classical finite element method to assess the reliability of the proposed method for modeling this complex instability problem.

Table 1
Normalized buckling parameters of a central cracked FGM plate for various values of gradient indices of material (n).

n	k_{uni}		
	Ref. [21]	Present study	Difference (%)
0.0	2.9995	3.0148	0.51
0.2	2.6548	2.6760	0.80
0.5	2.3470	2.3552	0.35
1.0	2.0977	2.1166	0.90
2.0	1.9222	1.9262	0.21
5.0	1.7825	1.7860	0.20
10.0	1.6751	1.6828	0.46

A dimensionless buckling load factor γ is defined as the ratio of the computed critical buckling stress of the cracked cylindrical shell (σ_{cr}) to the theoretical buckling stress of the perfect cylindrical shell subjected to axial compression (σ_{th}),

$$\gamma = \frac{\sigma_{cr}}{\sigma_{th}} \tag{43}$$

$$\sigma_{th} = \frac{E}{\sqrt{3(1-\nu^2)}}\left(\frac{t}{R}\right) \tag{44}$$

Also, another dimensionless loading parameter λ is defined as the ratio of the induced membrane stress due to internal pressure ($\sigma_{membrane}$) to the total axial compressive stress, developed due to internal pressure and axial compression (σ_{axial}), in the perfect cylindrical shell.

$$\lambda = \frac{\sigma_{membrane}}{\sigma_{axial}} \tag{45}$$

$$\sigma_{membrane} = \frac{pR}{t} \tag{46}$$

where p is the internal pressure applied on the inner surface of the cylinder.

First, an un-cracked cylindrical shell is considered and the effect of the internal pressure on the buckling stress associated with the first buckling mode is examined. It can be observed from Fig. 6 that with increasing the internal pressure the buckling stress increases slightly, which is consistent with the available results [13].

Then, an axially cracked cylindrical shell subjected to combined internal pressure and axial compression is considered and the critical buckling stresses are obtained for various internal pressures by the present method and then compared with available reference results [13], as plotted in Fig. 7. It is observed that, the computed buckling load parameters (γ) are in the very good agreement with the reference results [13]. It should be noted that, the number of elements was not mentioned in Ref. [13], so it is not possible to further compare the efficiency of the two methods. Moreover, it is observed that, for small crack length ratios ($a/R = 0.05$), with increasing the internal pressure, the buckling load parameter starts to increase, followed by a decreasing trend, showing the stabilizing effect of the internal pressure at low values. On contrary, for larger crack length ratios ($a/R = 0.1$), the internal pressure has a destabilizing effect on the buckling behavior of the cylinder, because with increasing the internal pressure, the buckling stress decreases.

To further examine the efficiency of the present XFEM formulation, a circumferentially cracked cylindrical shell ($\theta = 0^\circ$) subjected to combined internal pressure and axial compression [13] is considered. Variations of the computed buckling load parameter versus the internal pressure are compared with Ref. [13] in Fig. 8, which shows a good agreement. In contrast to the case of axial crack ($\theta = 90^\circ$), the internal pressure improves the local buckling behavior of cylinder due to its stabilizing effect on crack faces. Also, it is observed that for relatively long cracks, the effect of internal pressure is more significant on the buckling behavior of the cylindrical shell (Fig. 8).

3.2.2. Pure axial tensile load

A simply supported cracked cylindrical shell subjected to axial tension, recently studied by Seifi et al. [43], is considered. The material properties are $E = 70$ GPa and $\nu = 0.3$, and the geometric specifications are $L = 300$ mm, $R = 60$ mm, $t = 1.5$ mm, $\theta = 45^\circ$ and $a/R = 1.0$. A structured 35×45 (35 elements in the circumferential and 45 elements in the longitudinal direction) mesh is adopted for the analysis.

The critical buckling stress related to the first mode of buckling is predicted as $\sigma_{cr} = 231.9$ MPa, which is in good agreement with

the reference value of $\sigma = 231.81$ MPa. Ref. [43] used 3466 elements with 5 Gauss integration points in the thickness direction that leads to the total number of 17,330 Gauss points, which is far more than the total number of Gauss points and elements used in this study, since only two Gauss integration points considered across the thickness (1575 elements and 3150 Gauss points). The ability of the present method to capture the stress singularity at crack tips without refining the element size allows for higher accuracy and lower computational cost than the reference finite element solution [43], i.e. the approach employed for this particular case results in 5.5 times less computational cost.

3.3. Functionally graded cylindrical shells

After examining the accuracy and efficiency of the proposed XFEM in handling the problem of buckling of cracked homogeneous cylindrical shells, the method is now applied for modeling the more complex problem of buckling analysis of cracked functionally graded shells.

First, the problem of buckling analysis of an un-cracked FGM cylindrical shell under compressive load is considered and the validity of the proposed method is verified with available Ref. [44]. Then, the method is adopted for buckling analysis of cracked functionally graded cylindrical shells for three different cases of loading conditions; axial tension, axial compression and combined internal pressure and axial compression, as well as a compressive FGM cylindrical shell with three parallel cracks.

3.3.1. Uncracked FGM cylindrical shell subjected to axial compression

Consider a simply supported functionally graded cylindrical shell, which is subjected to axial compression, as depicted in Fig. 1. The length to the radius ratio of the shell is $L/R = 2$ and the effects of different radius to thickness ratios (R/t) and gradient index of the material (n) on the buckling behavior are investigated

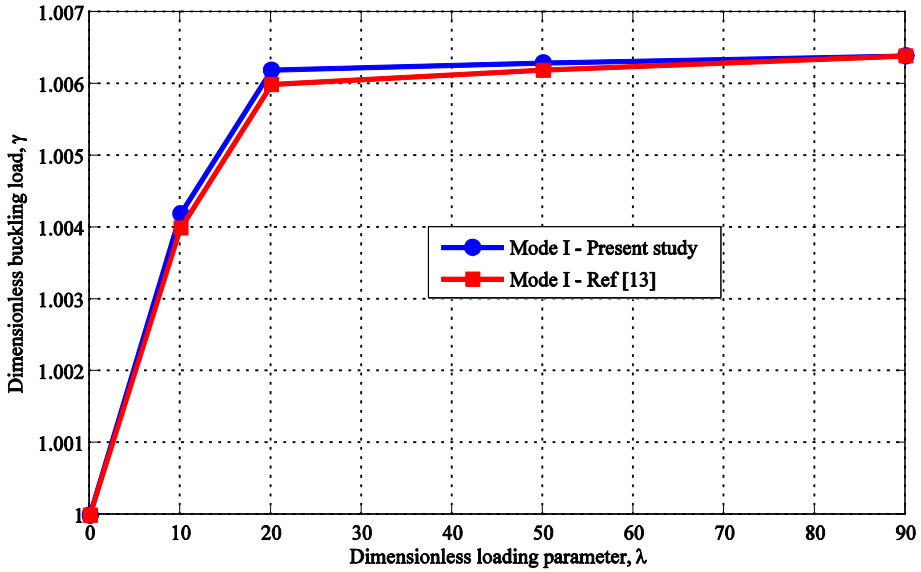

Fig. 6. Effect of the internal pressure on the buckling stress of the first buckling mode for the un-cracked cylindrical shell.

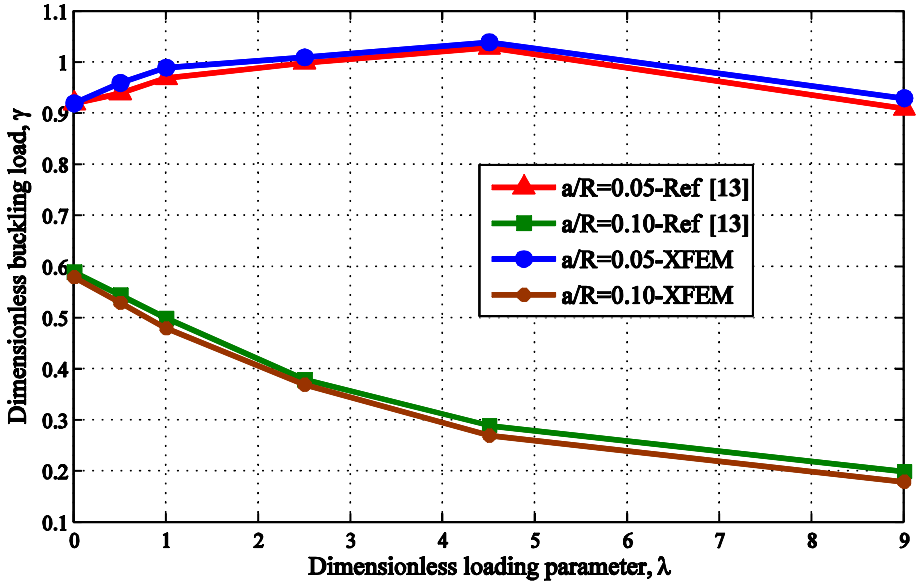

Fig. 7. Buckling load parameters versus internal pressure for axially cracked cylindrical shell.

by the present method and compared with the available reference results [44]. The material properties of the problem are $E_c = 3.8 \times 10^5$ MPa and $E_m = 7 \times 10^4$MPa on the ceramic and metallic sides of the FGM thickness, respectively, and the Poisson's ratio is considered constant across the thickness ($v = 0.3$).

Computed buckling stresses for various gradient indices are normalized by E_c and then plotted versus different radius to thickness ratios of the cylinder in Fig. 9. Clearly, the obtained results are very close to the reference results [44]. In addition, as the gradient index increases, the normalized buckling stress decreases significantly. Moreover, increasing the radius to thickness ratio affects the buckling behavior of the cylinder dramatically.

3.3.2. Cracked FGM cylindrical shell subjected to axial tension

In this section, the buckling analysis is carried out using the proposed XFEM method for extracting the critical buckling stress of a simply supported mixed-mode cracked functionally graded cylindrical shell under axial tension, as shown in Fig. 1. It should be noted that, under a uniform axial tensile load, a cracked cylindrical shell can buckle locally around the crack faces due to the generated compressive stress fields in these region. The material properties of the thin cylindrical shell is assumed similar to Section 3.3.1 and the length to radius ratio (L/R) and the radius to thickness ratio (R/t) of the shell are 4 and 1000, respectively.

All cracked FGM shells are modelled by a 45×55 structured mesh (45 elements in the longitudinal and 55 elements in the circumferential direction), unless otherwise mentioned. The effects of crack lengths and angles, gradient index of material, thickness and the length of the cylinder on the buckling behavior of the shell are investigated comprehensively. Also, the buckling mode shapes are presented to better illustrate the local instability of crack edges.

The tensile buckling stresses for different crack lengths and gradient indices for crack direction of $\theta = 0^\circ$ are presented in Table 2.

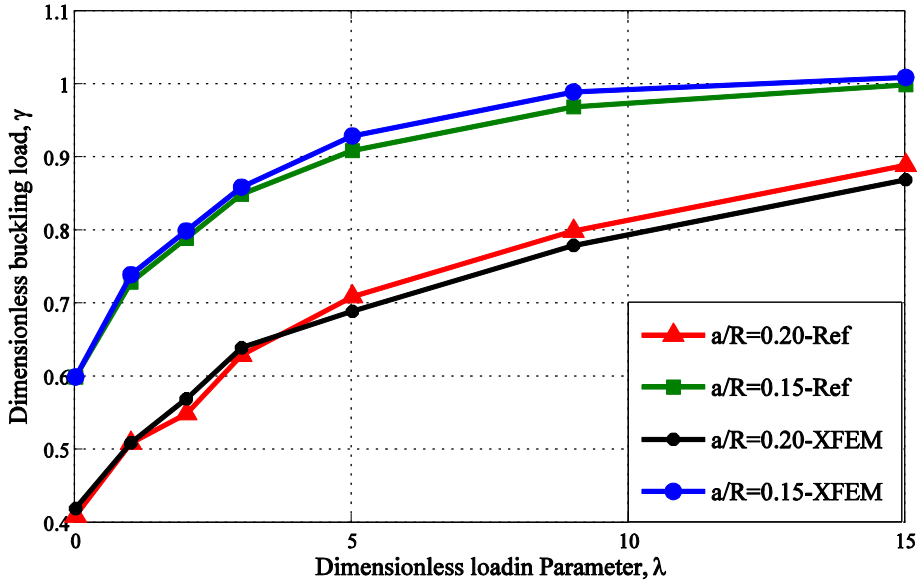

Fig. 8. Buckling load parameters versus internal pressure for circumferential cracked cylindrical shell.

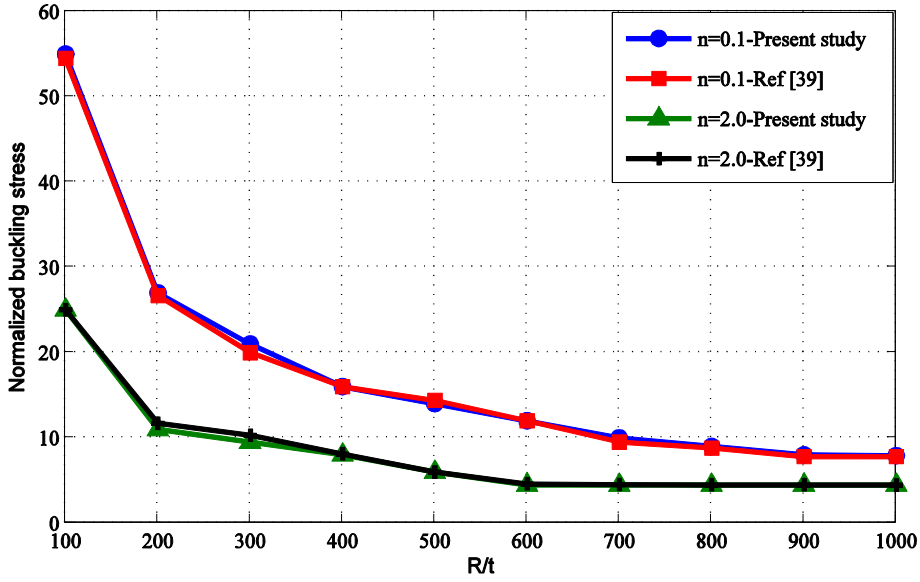

Fig. 9. Normalized buckling stress against the radius to thickness ratio for an uncracked FGM cylindrical shell subjected to axial compression.

It is observed that the predicted critical buckling stresses are so sensitive to the ratio of the crack length to radius of the shell, so that for the constant gradient index $n = 2$, the buckling stress dramatically decreases from 1675 MPa to 148 MPa when the ratio of the crack length to radius increases from 0.5 to 1.0. Furthermore, with increasing the gradient index of the material, the expected buckling stress decreases. For example, when the crack length to radius ratio is equal to 1.0 and the gradient index is $n = 0.5$, the buckling stress is approximately two times higher than its value for $n = 10$.

Table 2
Critical buckling stresses for various gradient indices and crack length to radius ratios for a circumferentially cracked FGM cylindrical shell subjected to axial tension.

a/R	n					
	0.5	1	2	4	6	10
	Critical buckling Stress (MPa)					
0.5	2717	2165	1675	1336	1194	1054
0.7	1397	1099	853	700	638	572
1.0	243	191	148	122	112	101
1.2	172	136	105	86	78	69

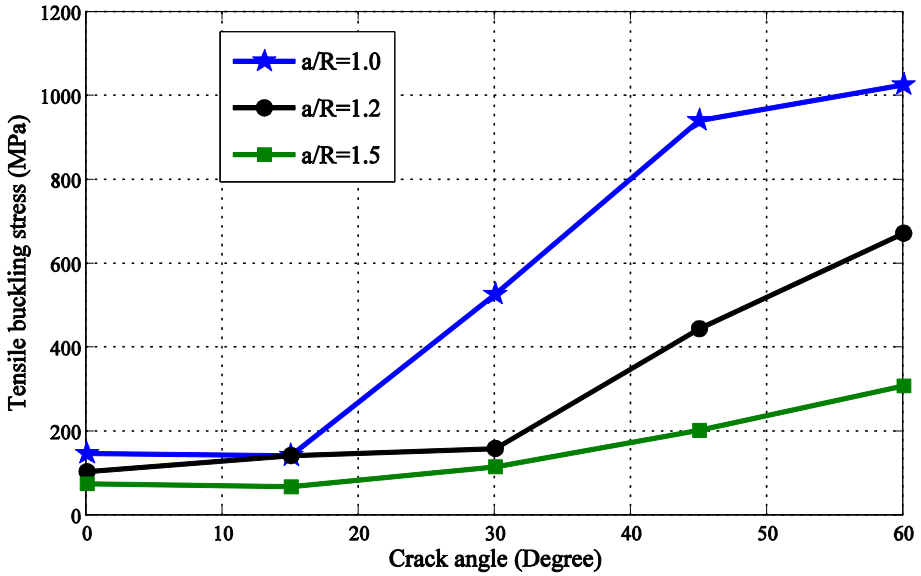

Fig. 10. Tensile buckling stresses for different crack angles for a FGM cylindrical shell.

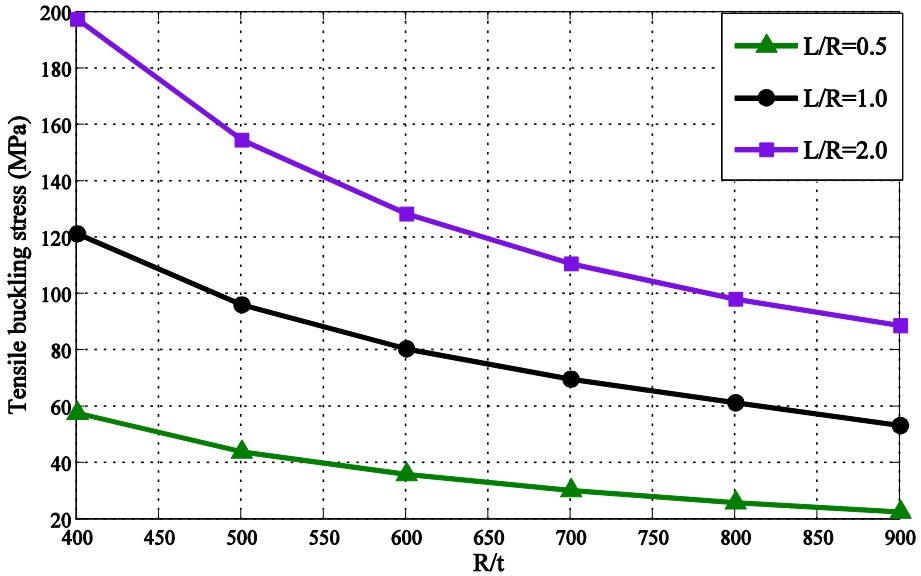

Fig. 11. Effect of the aspect ratio of the cracked FGM cylindrical shell on the critical tensile buckling stress.

For examining the effects of crack orientation on the buckling behavior of the problem, Fig. 10 compares the results for various crack angles for the constant gradient index of $n = 2.0$. Clearly, with increasing the crack angle, the buckling stress increases significantly. For instance, for the case of $a/R = 1.0$, the critical buckling stress for $\theta = 60^\circ$ is approximately 7 times greater than the buckling stress for $\theta = 0^\circ$.

Fig. 11 examines the effects of thickness and length of the cylinder on the critical buckling stress. The results are related to the case of $n = 4.0$ and $a/R = 1.0$. Accordingly, the length to radius

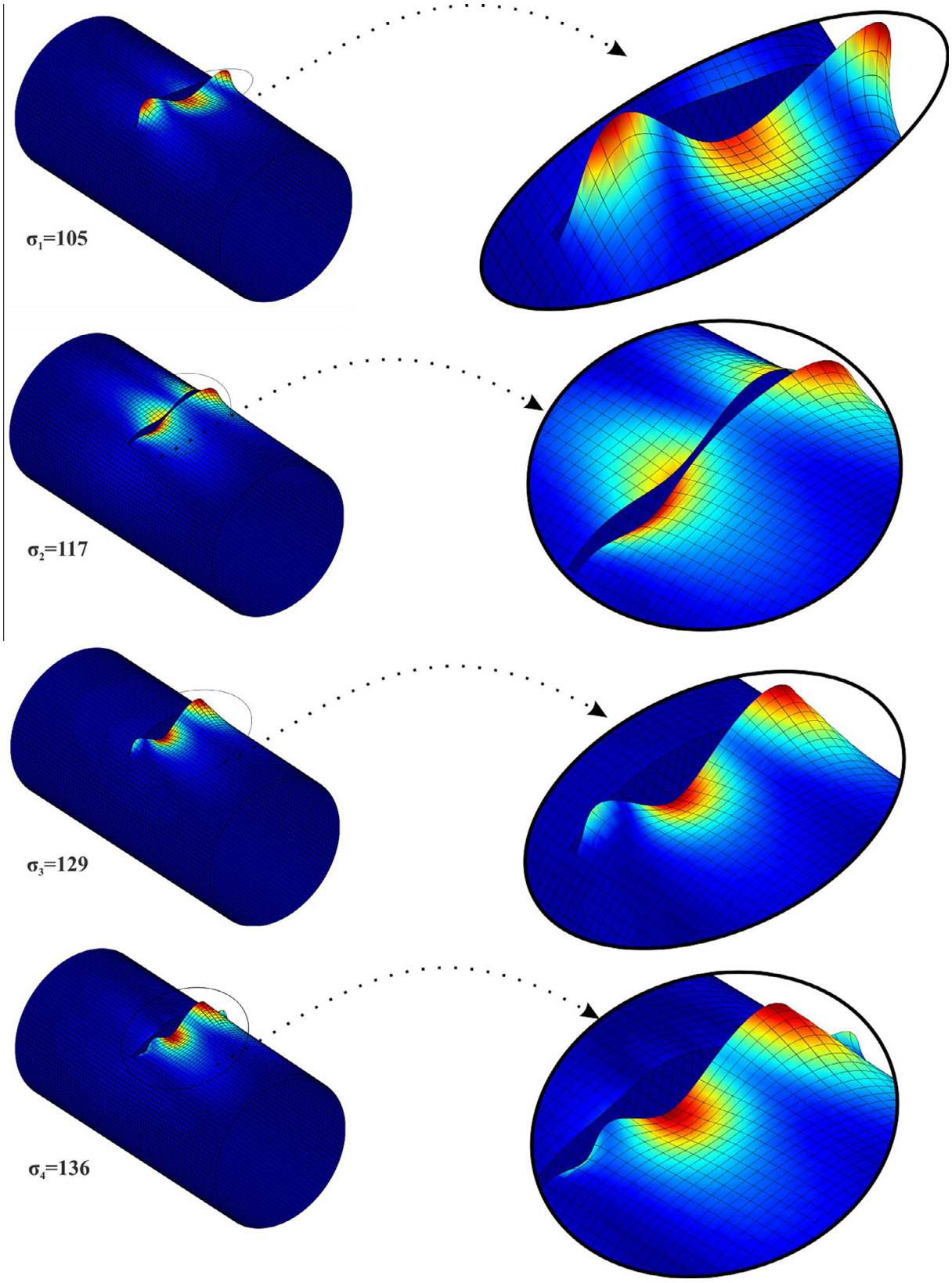

Fig. 12. The first three buckling mode shapes of the circumferentially cracked FGM cylindrical shell subjected to axial tension.

ratio of the cylinder highly affects the buckling behavior so that with decreasing the length to radius ratio the buckling stress significantly decreases. For instance, the buckling stress for the case of $L/R = 2.0$ and $R/t = 400$ is approximately 3.4 times greater than the case with the same thickness and $L/R = 0.5$. Clearly, the buckling stress is so sensitive to the radius to thickness ratios, where increasing the radius to thickness ratio leads to a considerable reduction in the buckling stress.

The buckling mode shapes related to the case of gradient index $n = 2$ and $a/R = 1.2$ are presented in Fig. 12. The local instability of crack edges are clearly observed in the Fig. 12. Higher critical stresses are obtained for the second and third modes of buckling.

Moreover, in order to investigate the sensitivity of the results to the number of elements, different number of meshes are adopted for the case of $a/R = 0.5$ and $n = 6.0$ and the buckling stresses are obtained. It is observed from the Fig. 13 that by increasing the number of elements, the buckling stress converges to 1197.63 MPa.

It is clearly demonstrated that cracked functionally graded cylindrical shells, even in the tensile loading condition, which is the safest loading state, are highly prone to local buckling around the crack faces. Moreover, even a slight increase in the crack length could substantially jeopardize the stability of the cylinder.

3.3.3. Cracked functionally graded cylindrical shell subjected to axial compression

Buckling analysis for cracked functionally graded cylindrical shell subjected to axial compression in general mixed-mode condition is now performed with the developed extended finite element method. Geometric parameters and material properties of the shell are similar to Section 3.3.2, unless mentioned otherwise. Besides, it is investigated that how different parameters such as crack lengths and orientations, gradient index of the material, thickness and the

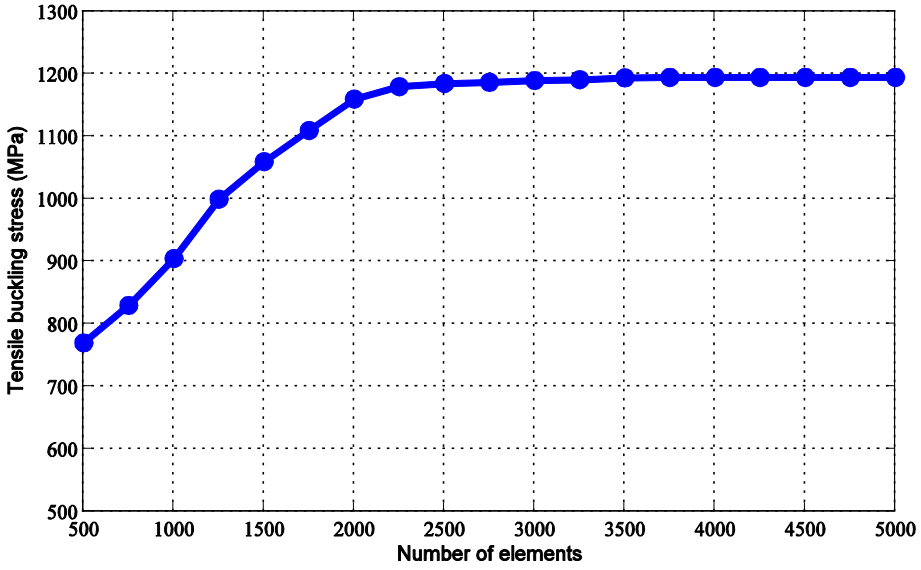

Fig. 13. Sensitivity of the buckling stress to the number of elements for the circumferential cracked FGM cylindrical shell subjected to axial tension.

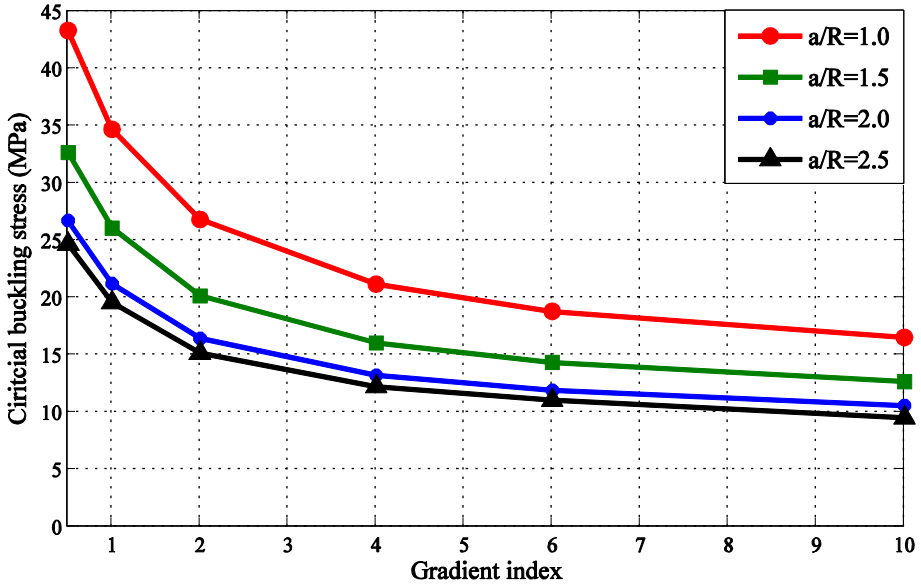

Fig. 14. Effects of the crack length ratios and the gradient index on the buckling stress of axial cracked FGM cylindrical shell under axial compression.

length of the shell can influence the buckling behavior of the FGM cylindrical shell.

First, the effects of crack length to radius ratio (a/R) and the gradient index of the material on an axially cracked ($\theta = 90^\circ$) FGM shell are examined. According to Fig. 14, different conclusions can be made. First, the crack length substantially affects the buckling behavior of the shell. For example, for the constant gradient index $n = 0.5$, the buckling stress related to $a/R = 1.0$ is decreased

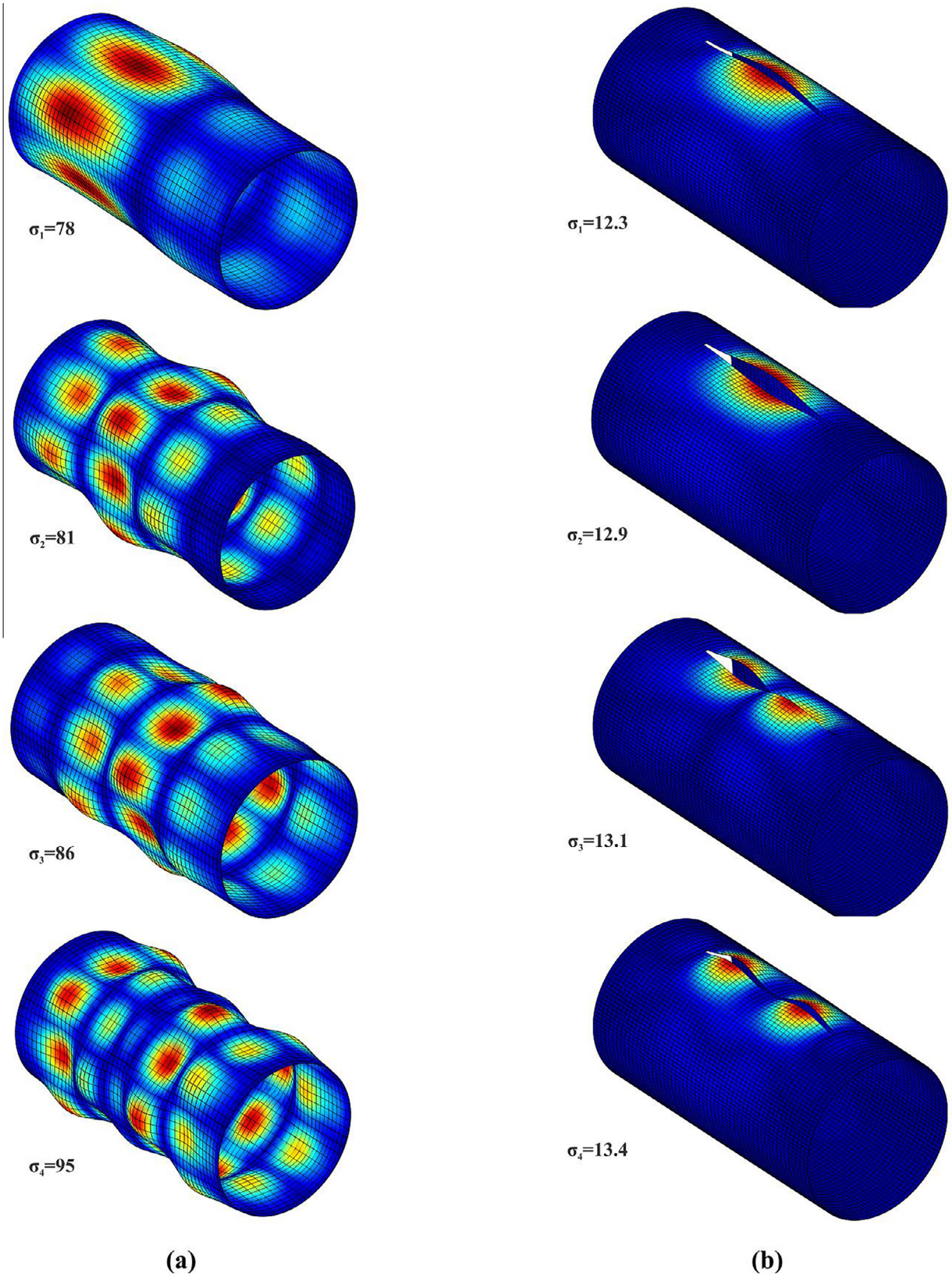

Fig. 15. The first four buckling mode shapes for (a) uncracked and (b) axially cracked functionally graded cylindrical shell subjected to axial compression.

significantly from 43.35 MPa to 24.72 MPa, associated with the crack length to radius ratio of $a/R = 2.5$. Then, the buckling stress can crucially be affected by the gradient index of the material, so higher increase of the gradient index leads to more reduction in the buckling stress. Also, it can be noted that for all cases of crack lengths, the buckling stresses for $n = 0.5$ are approximately 2.6 times greater than those in which $n = 10$.

To better illustrate how the presence of crack can alter the buckling behavior of the FGM cylindrical shell, the first four buckling mode shapes and their corresponding buckling stresses for uncracked and axially cracked FGM cylindrical shells are presented in Fig. 15. Clearly, existence of the crack can totally change the buckling behavior from the global buckling to local buckling around the crack faces in a very lower value of critical applied stress.

In order to investigate the influence of crack orientation on the buckling behavior of the problem, the critical compressive buckling stress for different crack lengths and orientations for the constant gradient index $n = 2.0$ are computed and depicted in Fig. 16. It is observed that variations of crack lengths and angles lead to different and complex buckling behaviors, making it impossible to make a general conclusion. Notwithstanding, for all a/R cases, the minimum critical buckling stress corresponds to the axial crack ($\theta = 90^\circ$).

Fig. 17 is given to probe the effects of aspect ratios of shell on the critical buckling stresses for $a/R = 0.8$, $n = 4.0$ and $\theta = 90^\circ$. Generally, with increasing the radius to thickness ratios (decreasing the thickness), the buckling stress decreases considerably. Nevertheless, the critical buckling stresses are not highly affected by variation of the length of the cylinder. For instance, for the case

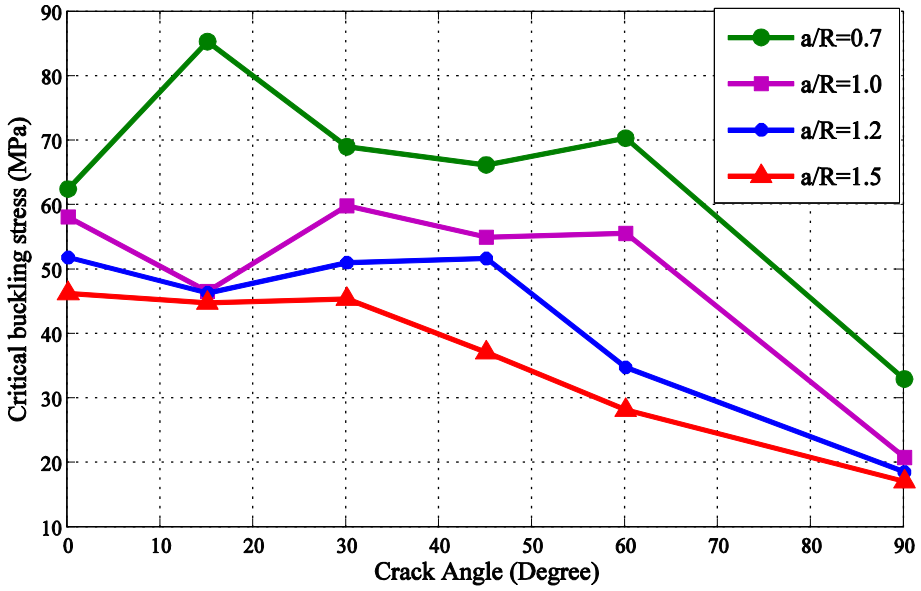

Fig. 16. Compressive buckling stresses for different crack lengths and angles.

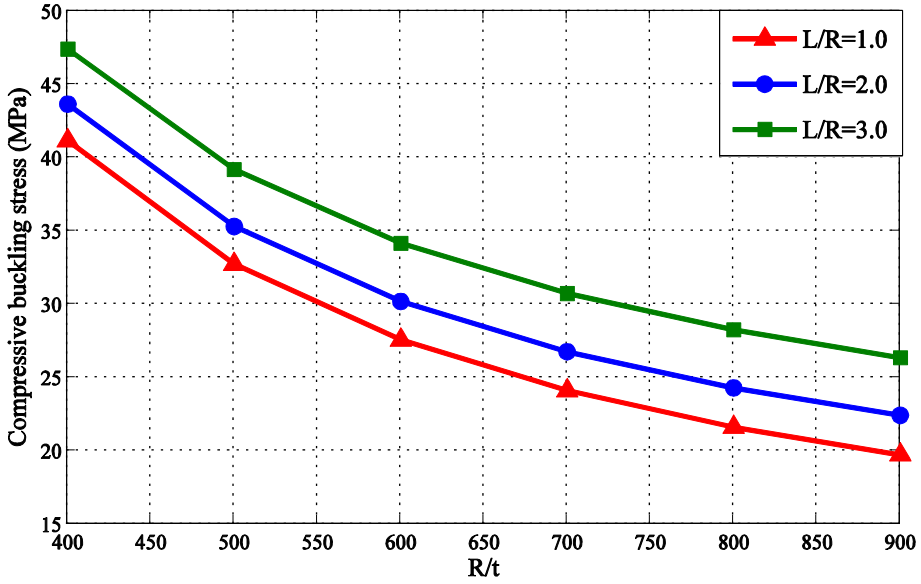

Fig. 17. Effects of aspect ratios on the critical buckling stresses of the axially cracked FGM cylindrical shell subjected to compression.

of $R/t = 400$, the buckling stress decreases about 15% when the length to radius ratio of the cylinder decreases from 3 to 1.

Also, Fig. 18 presents the influence of crack orientation and length of the shell on the buckling behavior. The first four buckling mode shapes and their associated buckling stresses for two different cases of $\theta = 15^\circ$ and $\theta = 30^\circ$ and the length to radius ratio of $L/R = 2$ and $R/t = 50$ are shown in Fig. 18. Based upon the plots given in Figs. 15 and 18, it is observed that any variations in crack

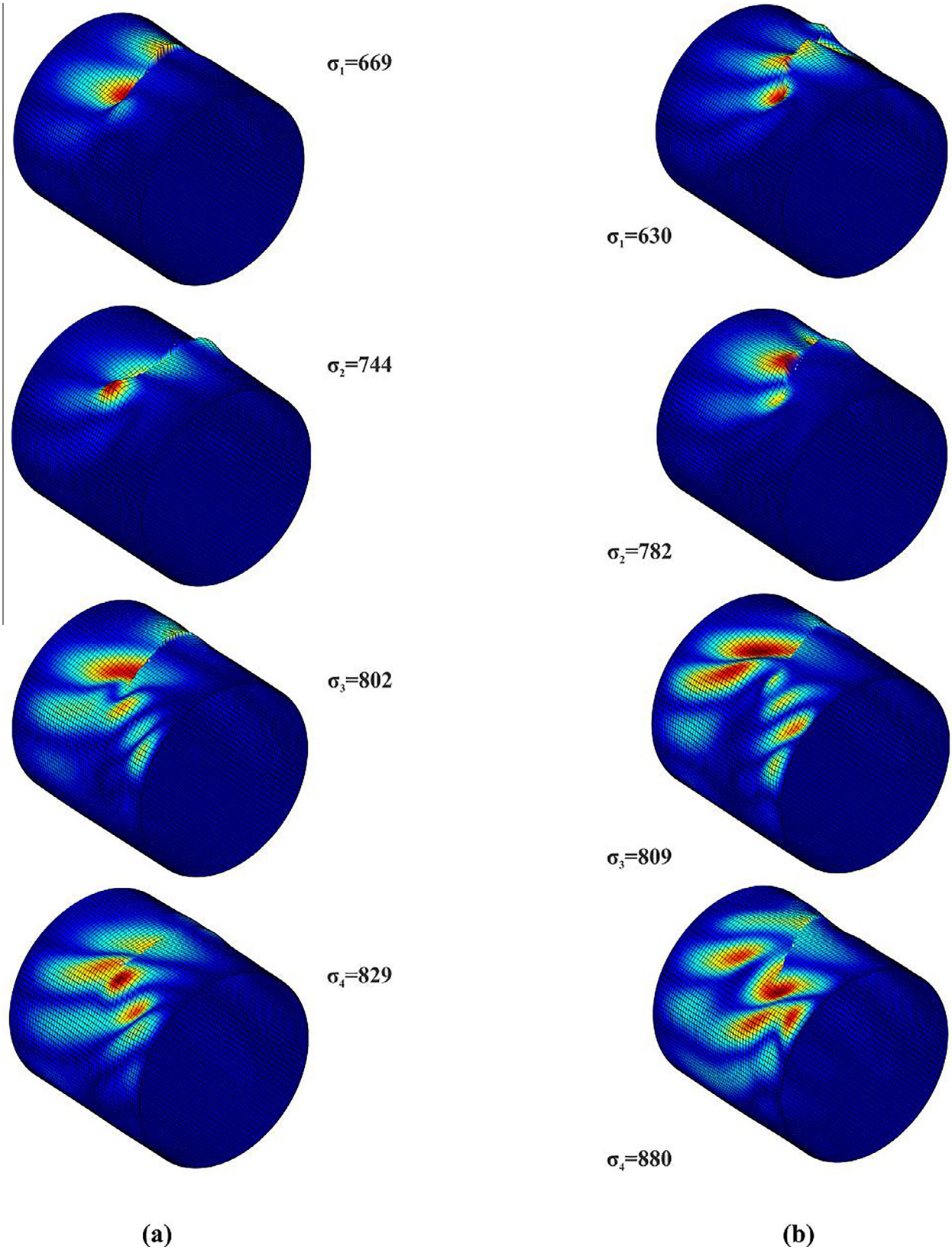

Fig. 18. The first four compressive buckling mode shapes for mixed-mode cracked FGM cylindrical shell a) $\theta = 15^\circ$ b) $\theta = 30^\circ$.

orientation or the geometrical parameters (L/R and R/t) severely alter the buckling behavior of the cracked FGM cylindrical shell.

3.3.4. Cracked functionally graded cylindrical shell subjected to combined internal pressure and axial compression

One of the dominant loading conditions in the cylindrical shells is when simultaneous axial compression and internal pressure are applied to the shell. This problem with homogeneous isotropic material was briefly studied in Section 3.2 and verified with the available results. Now, the problem is further extended to cracked FGM cylindrical shell and the buckling analysis is performed using the extended finite element method. The material properties and geometric parameters are identical to previous FGM examples and the shell is simply supported at the both ends.

Fig. 19 presents the effect of crack length to radius ratio and gradient index of the material on the critical internal pressure which causes buckling. It is observed that the critical internal pressure decreases significantly as the crack length ratios and gradient index increase.

Fig. 20 depicts the effects of internal pressure on the critical axial compressive buckling stresses for axially cracked functionally graded cylindrical shell in terms of various crack length to radius ratios for the constant value of $n = 2.0$. P_c denotes the critical internal pressure, computed in Fig. 19. It is observed that the internal pressure has a detrimental effect on the buckling behavior, where, with increasing the applied internal pressure, the axial buckling stress decreases dramatically. Also, for high values of internal pressure, buckling occurs at approximately the same axial compression for all crack lengths.

Now, the effect of internal pressure on the circumferential cracked FGM cylindrical shell is examined. According to Fig. 21, the critical buckling stress highly depends to the internal pressure.

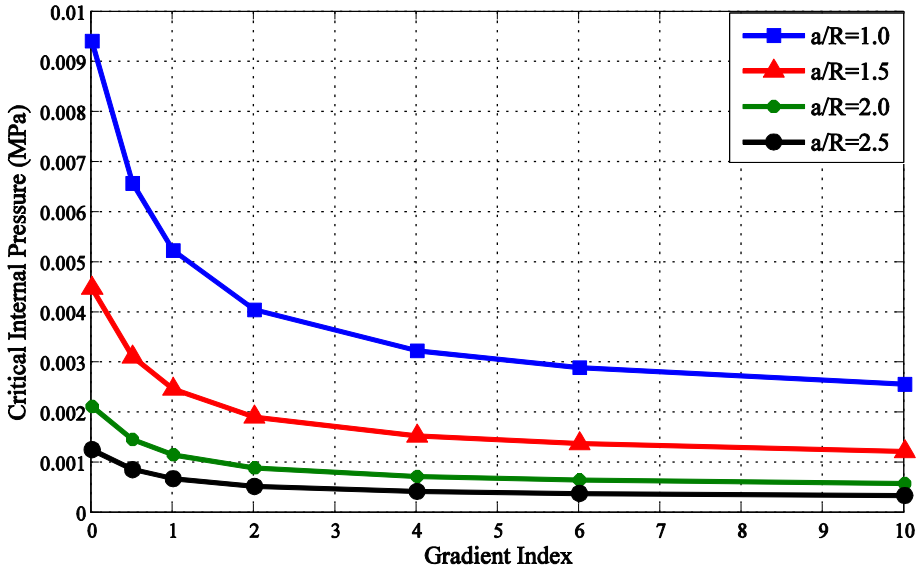

Fig. 19. Effects of gradient index and crack length ratios on the critical internal pressure for the axially cracked FGM cylindrical shell subjected to internal pressure.

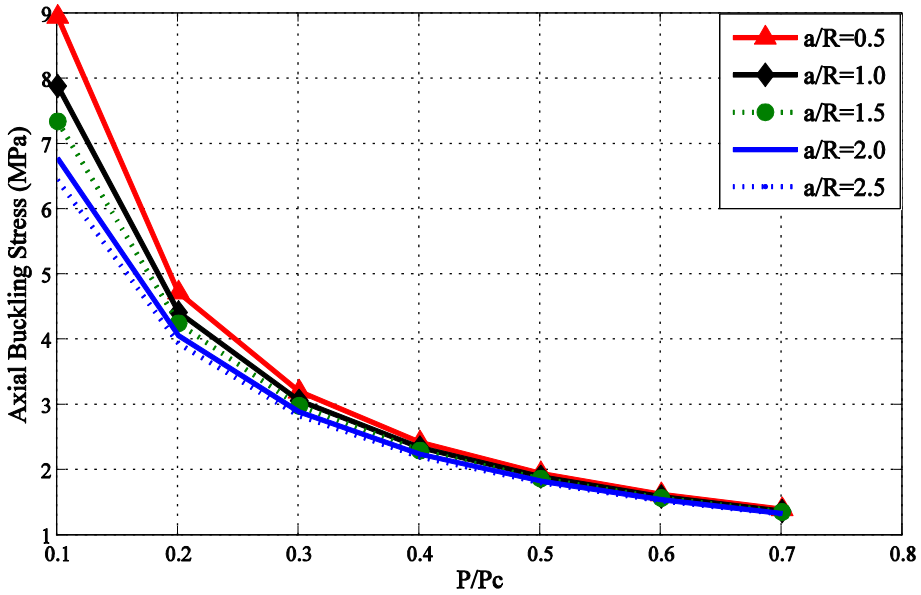

Fig. 20. Effect of internal pressure on the critical axial buckling stress for the axially cracked FGM cylindrical shell for different values of crack length ratios and $n = 2.0$.

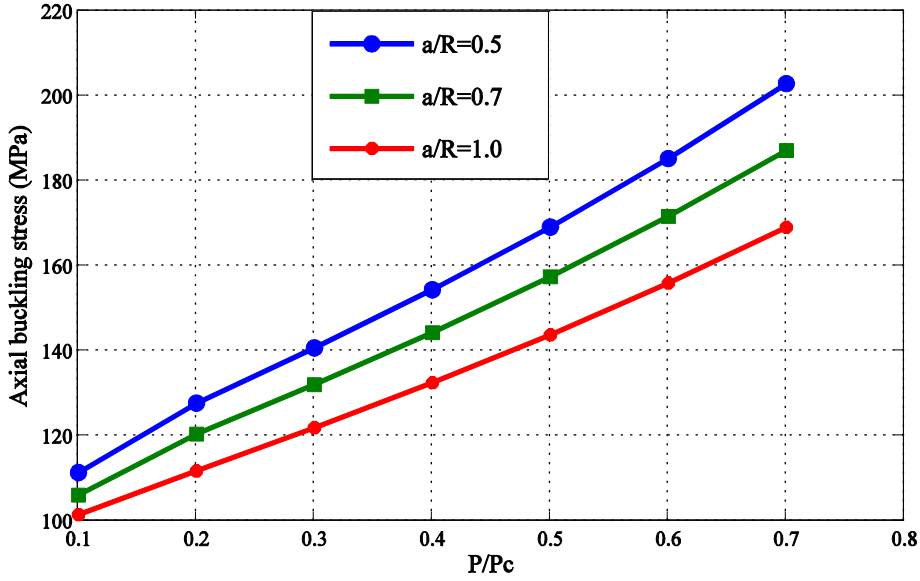

Fig. 21. Effects of internal pressure on the critical buckling stresses for circumferential cracked FGM cylindrical shell for different crack length ratios and $n = 2.0$.

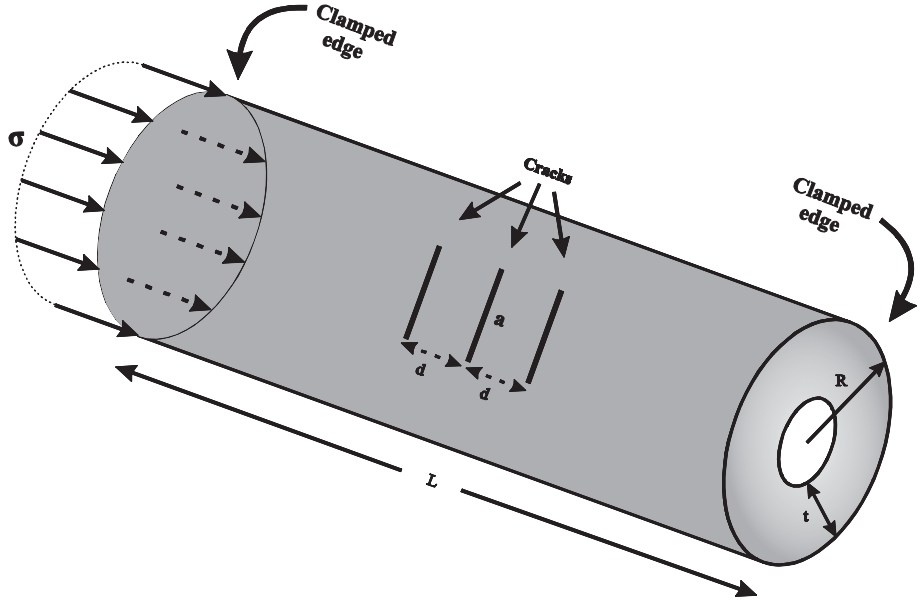

Fig. 22. An FGM cylindrical shell with three parallel cracks.

Table 3
Critical buckling stresses of an FGM cylindrical shell with three parallel cracks for various crack lengths and distances between cracks.

a/R	d/L				
	0.05	0.125	0.25	0.375	0.45
	Critical buckling stress (MPa)				
0.7	61.55	57.34	50.75	43.90	38.07
1.0	25.56	24.80	21.11	13.41	10.67
1.2	15.42	11.86	9.31	5.85	4.84
1.5	10.66	7.05	5.28	3.30	2.53

Also, it should be noted that, in contrast to the axially cracked cylinder, the internal pressure has a significant stabilizing effect on the buckling behavior of the circumferential cracked functionally graded cylindrical shell.

3.3.5. FGM cylindrical shell with multiple cracks subjected to axial compression

Compared with the conventional finite element method, one of the advantages of XFEM is its ability to model problems involving

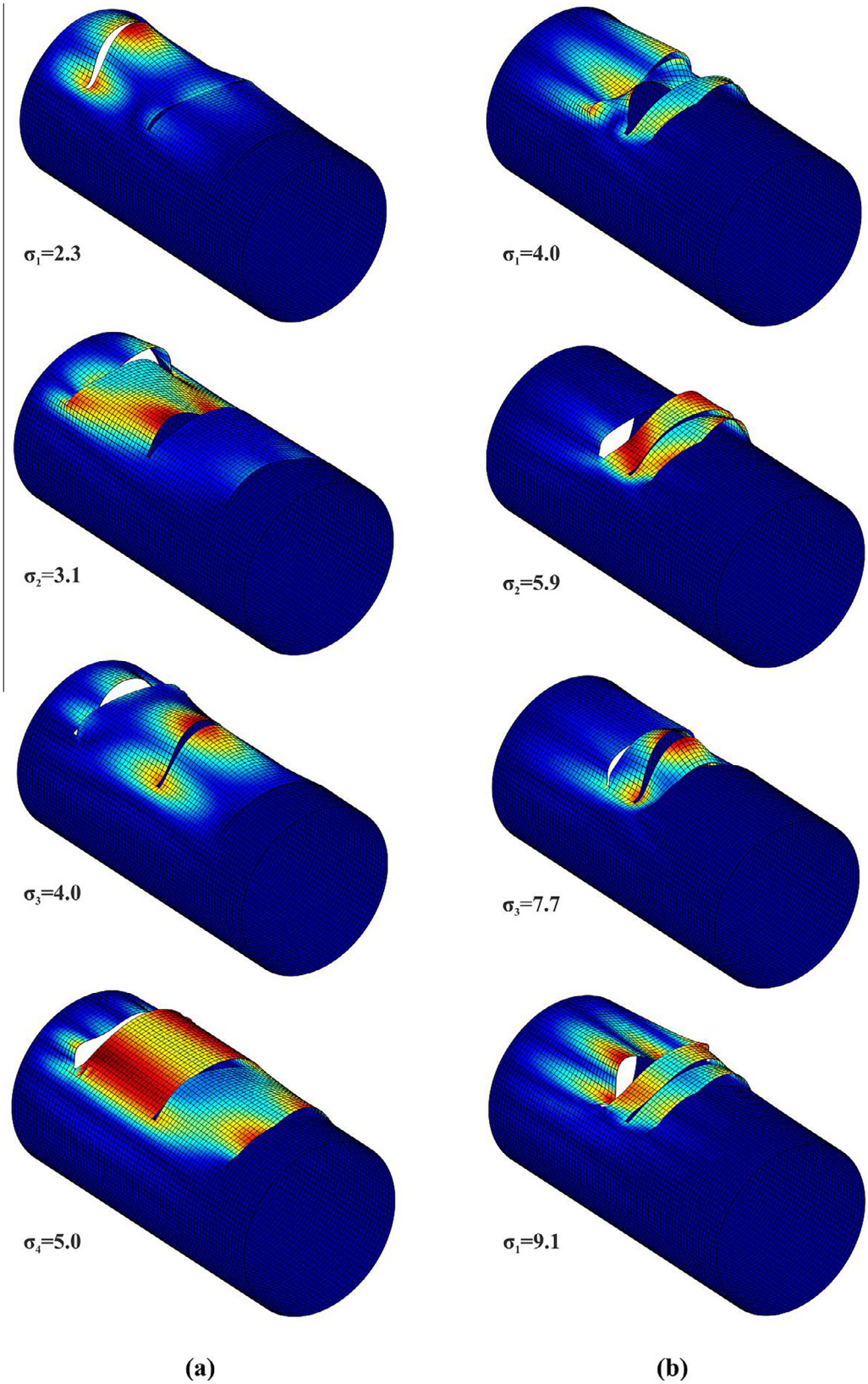

Fig. 23. The first four buckling mode shapes of the FGM cylindrical shell for two different values of d/L, a) $d/L = 1/3$ b) $d/L = 1/10$.

multiple cracks without noticeably altering the geometry of the mesh. Thereupon, as the last example, the buckling behavior of an FGM shell with three parallel cracks subjected to compression, as depicted in Fig. 22, is investigated. Geometric and material properties of the shell is identical to those in the previous examples. Also, the shell is clamped at both ends. The effect of the distances between the cracks on the critical buckling stress and the corresponding mode shapes are probed.

For investigating the effects of crack length and distance between cracks, critical buckling stresses associated with $n = 2.0$ are obtained and presented in Table 3. Clearly, the buckling stresses are drastically decreased by increase of crack lengths. For instance, in the case of $d/L = 0.05$, the buckling stress for $a/R = 1.5$ is 6 times greater than the case associated with $a/R = 0.7$. Besides, the buckling behavior of shell is affected by the variation of distance between cracks, so that the buckling stress decreases when the distance between cracks increease. For example, in the case of $a/R = 1.5$, the buckling stress for $d/L = 0.45$ is 3 times smaller than the case in which $d/L = 0.05$.

The buckling mode shapes related to $d/L = 1/10$and$d/L = 1/3$ and their associated buckling stresses for the crack length to radius ratio $a/R = 1.5$ and $n = 0.5$ are depicted in Fig. 23. Clearly, the distances between the cracks can crucially alter the buckling behavior of the shell.

4. Conclusion

A comprehensive study on the buckling behavior of cracked FGM cylindrical shells has been performed by the extended finite element method to numerically solve the stability equation. First, the method has been verified by the analysis of reference cracked isotropic cylindrical shells. It has been illustrated that not only the present XFEM formulation is accurate enough, it is also computationally more efficient than the conventional finite element method. From the computational cost standpoint, the work presented herein is several times more efficient compared with, for example, the work done by Seifi et al. [43]. Then, the method has been implemented to analyze the buckling behavior of a cracked FGM cylindrical shell under three different loading conditions and also an FGM cylindrical shell with three parallel cracks under axial compression. The effects of several parameters such as crack lengths and angles, aspect ratios of the shell and the gradient index of the material on the buckling behavior of the problem have been examined thoroughly.

Some of the most important conclusions of the study can be outlined as follows:

In general, as the length of the crack increases, the critical buckling stress of the shell drops. The same conclusion can be made about the gradient index of the functionally graded material (n). Thus, the value of the critical buckling stress of the FGM cylindrical shell is highly depends on the aforementioned parameters.

- The buckling behavior of the FGM shell is under the severe influence of the angle of the crack (θ). So much so that in tension, as the angle of the crack heightens, the critical buckling stress of the shell noticeably increases, whereas in compression, due to the complex nature of the mechanics of the problem, a definite conclusion cannot be made. Nevertheless, for $\theta = 90^\circ$, the critical buckling stress is minimized.
- It is obvious that the thickness of the FGM shell can greatly affect the critical buckling stress of the FGM shell.
- The length of the shell, also, plays an important role in the buckling behavior of the FGM shell. As the length of the shell decreases, the buckling stress of the shell experiences a drop. This assertion can be attributed to both tensile and compressive external loads. But the effect is much more strongly felt in tension.
- The effect of the internal pressure on the buckling of shell has been thoroughly investigated for two different crack angles ($\theta = 0^\circ$ and $\theta = 90^\circ$). It was observed that when crack is along the axis of the shell, the increase in the internal pressure of the FGM shell results in a significant reduction in the buckling stress. For $\theta = 0^\circ$, the internal pressure in the FGM shell exerts a stabilizing effect on the critical buckling stress. i.e. as the internal pressure increases, the buckling stress increase as well.

Acknowledgements

The authors wish to gratefully acknowledge the technical support of the High Performance Computing Lab, School of Civil Engineering, University of Tehran. Also, the first author would like to extend his gratitude to Dr Hamid Bayesteh for his invaluable contributions which improved the quality of the present research. Furthermore, the financial support of Iran National Science Foundation (INSF) is gratefully acknowledged.

References

[1] Ng T, Lam K, Liew K, Reddy J. Dynamic stability analysis of functionally graded cylindrical shells under periodic axial loading. Int J Solids Struct 2001;38:1295–309.
[2] Sofiyev A. The stability of compositionally graded ceramic–metal cylindrical shells under aperiodic axial impulsive loading. Compos Struct 2005;69:247–57.
[3] Bagherizadeh E, Kiani Y, Eslami M. Mechanical buckling of functionally graded material cylindrical shells surrounded by Pasternak elastic foundation. Compos Struct 2011;93:3063–71.
[4] Huang H, Han Q. Nonlinear dynamic buckling of functionally graded cylindrical shells subjected to time-dependent axial load. Compos Struct 2010;92:593–8.
[5] Shariyat M. Dynamic thermal buckling of suddenly heated temperature-dependent FGM cylindrical shells, under combined axial compression and external pressure. Int J Solids Struct 2008;45:2598–612.
[6] Shen H-S. Postbuckling analysis of pressure-loaded functionally graded cylindrical shells in thermal environments. Eng Struct 2003;25:487–97.
[7] Shen H-S. Thermal postbuckling behavior of functionally graded cylindrical shells with temperature-dependent properties. Int J Solids Struct 2004;41:1961–74.
[8] Shen H-S, Noda N. Postbuckling of FGM cylindrical shells under combined axial and radial mechanical loads in thermal environments. Int J Solids Struct 2005;42:4641–62.
[9] Shen H-S, Noda N. Postbuckling of pressure-loaded FGM hybrid cylindrical shells in thermal environments. Compos Struct 2007;77:546–60.
[10] Wu L, Jiang Z, Liu J. Thermoelastic stability of functionally graded cylindrical shells. Compos Struct 2005;70:60–8.
[11] Estekanchi H, Vafai A. On the buckling of cylindrical shells with through cracks under axial load. Thin-Walled Struct 1999;35:255–74.
[12] Vafai A, Estekanchi H. A parametric finite element study of cracked plates and shells. Thin-walled Struct 1999;33:211–29.
[13] Vaziri A, Estekanchi H. Buckling of cracked cylindrical thin shells under combined internal pressure and axial compression. Thin-Walled Struct 2006;44:141–51.
[14] Vaziri A. On the buckling of cracked composite cylindrical shells under axial compression. Compos Struct 2007;80:152–8.
[15] Javidruzi M, Vafai A, Chen J, Chilton J. Vibration, buckling and dynamic stability of cracked cylindrical shells. Thin-Walled Struct 2004;42:79–99.
[16] Tafreshi A. Efficient modelling of delamination buckling in composite cylindrical shells under axial compression. Compos Struct 2004;64:511–20.
[17] Tafreshi A. Delamination buckling and postbuckling in composite cylindrical shells under combined axial compression and external pressure. Compos Struct 2006;72:401–18.
[18] Tafreshi A. Instability of delaminated composite cylindrical shells under combined axial compression and bending. Compos Struct 2008;82:422–33.
[19] Nasirmanesh A, Mohammadi S. XFEM buckling analysis of cracked composite plates. Compos Struct 2015;131:333–43.
[20] Natarajan S, Chakraborty S, Ganapathi M, Subramanian M. A parametric study on the buckling of functionally graded material plates with internal discontinuities using the partition of unity method. Eur J Mech A/Solids 2014;44:136–47.
[21] Liu P, Bui T, Zhu D, Yu T, Wang J, Yin S, et al. Buckling failure analysis of cracked functionally graded plates by a stabilized discrete shear gap extended 3-node triangular plate element. Compos B Eng 2015;77:179–93.
[22] Baiz P, Natarajan S, Bordas S, Kerfriden P, Rabczuk T. Linear buckling analysis of cracked plates by SFEM and XFEM. J Mech Mater Struct 2012;6:1213–38.
[23] Afshar A, Daneshyar A, Mohammadi S. XFEM analysis of fiber bridging in mixed-mode crack propagation in composites. Compos Struct 2015;125:314–27.
[24] Ardakani SH, Afshar A, Mohammadi S. Numerical study of thermo-mechanical coupling effects on crack tip fields of mixed-mode fracture in pseudoelastic shape memory alloys. Int J Solids Struct 2015.
[25] Ardakani SH, Ahmadian H, Mohammadi S. Thermo-mechanically coupled fracture analysis of shape memory alloys using the extended finite element method. Smart Mater Struct 2015;24:045031.

[26] Asadpoure A, Mohammadi S. Developing new enrichment functions for crack simulation in orthotropic media by the extended finite element method. Int J Numer Meth Eng 2007;69:2150–72.
[27] Asadpoure A, Mohammadi S, Vafai A. Crack analysis in orthotropic media using the extended finite element method. Thin-Walled Struct 2006;44:1031–8.
[28] Asadpoure A, Mohammadi S, Vafai A. Modeling crack in orthotropic media using a coupled finite element and partition of unity methods. Finite Elem Anal Des 2006;42:1165–75.
[29] Belytschko T, Moës N, Usui S, Parimi C. Arbitrary discontinuities in finite elements. Int J Numer Meth Eng 2001;50:993–1013.
[30] Motamedi D, Mohammadi S. Dynamic crack propagation analysis of orthotropic media by the extended finite element method. Int J Fract 2010;161:21–39.
[31] Afshar A, Ardakani SH, Mohammadi S. Transient analysis of stationary interface cracks in orthotropic bi-materials using oscillatory crack tip enrichments. Compos Struct 2016.
[32] Ashari S, Mohammadi S. Delamination analysis of composites by new orthotropic bimaterial extended finite element method. Int J Numer Meth Eng 2011;86:1507–43.
[33] Bayesteh H, Mohammadi S. XFEM fracture analysis of orthotropic functionally graded materials. Compos B Eng 2013;44:8–25.
[34] Rashetnia R, Mohammadi S. Finite strain fracture analysis using the extended finite element method with new set of enrichment functions. Int J Numer Meth Eng 2015;102:1316–51.
[35] Nguyen-Thanh N, Valizadeh N, Nguyen M, Nguyen-Xuan H, Zhuang X, Areias P, et al. An extended isogeometric thin shell analysis based on Kirchhoff-Love theory. Comput Methods Appl Mech Eng 2015;284:265–91.
[36] Rabczuk T, Areias P. A meshfree thin shell for arbitrary evolving cracks based on an extrinsic basis; 2006.
[37] Rabczuk T, Areias P, Belytschko T. A meshfree thin shell method for non-linear dynamic fracture. Int J Numer Meth Eng 2007;72:524–48.
[38] Amiri F, Millán D, Shen Y, Rabczuk T, Arroyo M. Phase-field modeling of fracture in linear thin shells. Theoret Appl Fract Mech 2014;69:102–9.
[39] Areias P, Rabczuk T, Msekh M. Phase-field analysis of finite-strain plates and shells including element subdivision. Comput Methods Appl Mech Eng 2016.
[40] Bayesteh H, Mohammadi S. XFEM fracture analysis of shells: the effect of crack tip enrichments. Comput Mater Sci 2011;50:2793–813.
[41] Mohammadi S. Extended finite element method: for fracture analysis of structures. John Wiley & Sons; 2008.
[42] Cook RD. Concepts and applications of finite element analysis. John Wiley & Sons; 2007.
[43] Seifi R, Googarchin HS, Farrokhi M. Buckling of cracked cylindrical panels under axially compressive and tensile loads. Thin-Walled Struct 2015;94:457–65.
[44] Hajlaoui A, Jarraya A, El Bikri K, Dammak F. Buckling analysis of functionally graded materials structures with enhanced solid-shell elements and transverse shear correction. Compos Struct 2015.